



Published in final edited form as:

*Nat Neurosci.* 2020 September ; 23(9): 1111–1124. doi:10.1038/s41593-020-0675-x.

## Posterior Amygdala Regulates Sexual and Aggressive Behaviors in Male Mice

Takashi Yamaguchi<sup>1,\*</sup>, Dongyu Wei<sup>1</sup>, Soomin C. Song<sup>1</sup>, Byungkook Lim<sup>4</sup>, Nicolas X. Tritsch<sup>1</sup>, Dayu Lin<sup>1,2,3,\*</sup>

<sup>1</sup>Neuroscience Institute, New York University Langone Medical Center, New York, New York, USA

<sup>2</sup>Department of Psychiatry, New York University Langone Medical Center, New York, New York, USA

<sup>3</sup>Center for Neural Science, New York University, New York, New York, USA

<sup>4</sup>Neurobiology Section, Division of Biological Sciences, University of California San Diego, La Jolla, California, USA

### Abstract

Sexual and aggressive behaviors are fundamental to animals' survival and reproduction. The medial preoptic nucleus (MPN) and ventrolateral part of ventromedial hypothalamus (VMHvl) are essential regions for male sexual and aggressive behaviors, respectively. While key inhibitory inputs to VMHvl and MPN are identified, the extra-hypothalamic excitatory inputs essential for the social behaviors remain elusive. Here we identify estrogen receptor alpha (Esr1) expressing cells in posterior amygdala (PA) as a main source of excitatory inputs to hypothalamus and key mediators for mating and fighting in male mice. We find two largely distinct PA subpopulations that differ in connectivity, gene expression, *in vivo* responses and social behavior relevance. MPN projecting PA<sup>Esr1+</sup> cells are activated during mating and necessary and sufficient for male sexual behaviors, while VMHvl projecting PA<sup>Esr1+</sup> are excited during inter-male aggression and promote attacks. These findings place PA as a key node in both male aggression and reproduction circuits.

### Introduction

Social behaviors, such as mating and fighting, are essential for the survival of individuals and the propagation of species. Decades of research, mainly in rodents, identified several key hypothalamic regions essential for social behaviors<sup>1–12</sup>. The medial preoptic nucleus (MPN) is indispensable for male sexual behaviors. Lesion, ablation, chemical and

Users may view, print, copy, and download text and data-mine the content in such documents, for the purposes of academic research, subject always to the full Conditions of use:[http://www.nature.com/authors/editorial\\_policies/license.html#terms](http://www.nature.com/authors/editorial_policies/license.html#terms)

\*Corresponding Authors: [takashi.yamaguchi@nyulangone.org](mailto:takashi.yamaguchi@nyulangone.org); [dayu.lin@nyulangone.org](mailto:dayu.lin@nyulangone.org).

Author Contributions

D.L. conceived the project, designed experiments, analyzed data, and wrote the paper. T.Y. co-designed and performed most experiments, analyzed data and co-wrote the paper. D.W. and S.C.S. performed slice recording and analyzed data. N.X.T. supervised the slice recording experiment, analyzed data, and edited the paper. B.L. generated AAV-Ef1 $\alpha$ -fDIO-hM4Di-mCherry and AAV-Ef1 $\alpha$ -fDIO-hM3Dq-mCherry.

Competing interests

The authors declare no competing interests.

optogenetic inactivation of MPN consistently suppress male sexual behaviors while sex hormone supplement, electrical, chemical and optogenetic activation facilitate mating<sup>1-5</sup>. In contrast, the ventrolateral part of the ventromedial hypothalamus (VMHvl) is essential for inter-male aggression. Ablation or inactivation of VMHvl cells suppresses natural aggression whereas electric, pharmacogenetic and optogenetic activation elicits immediate attack towards both natural and suboptimal targets, e.g. inanimate objects<sup>6-10</sup>. Despite our growing appreciation for the role of hypothalamus in social behaviors, the aggression and mating circuits that lie beyond the hypothalamus remain incompletely understood.

Early retrograde tracing revealed that the amygdala and bed nucleus stria terminalis (BNST) are major upstream regions of MPN and VMHvl. Within the amygdala, the medial amygdala (MeA) has received much attention given its dense inputs from the accessory olfactory bulb, a region dedicated for processing pheromones<sup>13-19</sup>. Immediate early gene mappings and *in vivo* recordings demonstrated increased activity of MeA cells to conspecific olfactory cues although MeA cell responses during sexual and aggressive behaviors remain unreported<sup>13,16,20,21</sup>. Recent functional studies with precise targeting of the posterodorsal part of MeA (MeApd) revealed that GABAergic MeApd cells promote aggression but not sexual behaviors<sup>14,17</sup>. The principal part of BNST (BNSTpr) projects densely to both MPN and VMHvl<sup>22</sup>. Optical recording from BNSTpr aromatase expressing cells revealed their high activity during male sexual behaviors. Suppressing or killing the cells impairs preferences of female pheromone and sexual behaviors in males<sup>23</sup>. Noticeably, MeApd and BNSTpr contain mainly GABAergic cells and thus presumably provide primarily inhibitory inputs to MPN and VMHvl<sup>14,23</sup>.

Are the excitatory inputs to the MPN and VMHvl important for social behaviors? An early study demonstrates that L-glutamate infusion into the hypothalamus can elicit attack in cats<sup>24</sup>. Microdialysis in MPN reveals gradual increase of glutamate over the course of male sexual behaviors<sup>25</sup>. Infusion of glutamate uptake inhibitors into MPN facilitates copulations<sup>25</sup>. These early findings suggest that excitatory glutamatergic inputs to the medial hypothalamus are essential for both sexual and aggressive behaviors. What are the sources of excitatory inputs to medial hypothalamus? Anatomical tracing revealed that the posterior amygdala (PA), sometimes known as amygdalo-hippocampal area (AHA)<sup>26</sup> as one candidate source. PA is considered as a part of the cortical-like amygdala complex<sup>27,28</sup> and is largely glutamatergic (<http://mouse.brain-map.org/experiment/show/70436317>). Moreover, similar to MPN and VMHvl<sup>7,29,30</sup>, PA is enriched for estrogen receptor alpha (Esr1) (<http://mouse.brain-map.org/experiment/show/79591677>)<sup>31</sup>. Estrogen has a profound impact on social behaviors<sup>32</sup>. Thus, regions with abundant estrogen receptors are likely to be relevant for social behaviors. Indeed, c-Fos, a surrogate of neural activity, increased in PA after male aggression and sexual behaviors<sup>20,33</sup> although PA's function and *in vivo* responses remain largely unknown. Here, we use MPN and VMHvl as our entry points to examine the functions of Esr1<sup>+</sup> cells in PA (PA<sup>Esr1+</sup>) in controlling sexual and aggressive behaviors in male mice.

## Results

### Male PA cells that project to MPN and VMHvl are largely distinct

Since MPN and VMHvl contribute to different social behaviors, we hypothesized that PA neurons that project to MPN and VMHvl likely non-identical and play differentially roles in male sexual and aggressive behaviors. To test this, we first injected a retrograde tracer into the MPN or VMHvl of male mice and found that labeled cells distribute differently within PA. MPN-projecting PA cells (PA<sup>MPN</sup>) are abundant in the anterior dorsomedial part (Fig. 1a, b, e), whereas VMHvl projectors (PA<sup>VMHvl</sup>) concentrate in ventrolateral PA throughout the anterior-posterior axis (Fig. 1c–e). Additionally, both PA<sup>MPN</sup> and PA<sup>VMHvl</sup> cells preferentially overlap with *Esr1*<sup>+</sup> cells: nearly all PA<sup>MPN</sup> cells express *Esr1* ( $95.5 \pm 1.1\%$ ,  $n = 3$  animals) while approximately half of PA<sup>VMHvl</sup> cells contain *Esr1* ( $55.6 \pm 2.5\%$ ,  $n = 3$  animals; Fig. 1f).

To compare PA<sup>MPN</sup> and PA<sup>VMHvl</sup> cells in the same animals, we injected Alexa647 conjugated CTB into the VMHvl and Alexa555-CTB into the MPN and found the PA<sup>VMHvl</sup> and PA<sup>MPN</sup> cells are largely distinct at the single cell level. Among all PA cells,  $16.7 \pm 1.5\%$  are retrogradely labeled from MPN,  $22.2 \pm 3.0\%$  from VMHvl and only  $3.3 \pm 0.7\%$  are labeled from both regions ( $n = 3$  animals). The dual-labeled cells are largely located in the middle zone where PA<sup>MPN</sup> and PA<sup>VMHvl</sup> cells converge (Fig. 1g–j). To further visualize MPN-projecting PA<sup>Esr1+</sup> (PA<sup>Esr1+MPN</sup>) and VMHvl-projecting PA<sup>Esr1+</sup> (PA<sup>Esr1+VMHvl</sup>) cells, we injected a retrograde herpes simplex virus (HSV) encoding a *Cre*-dependent red fluorescent protein (HSV-hEfl $\alpha$ -LS1L-mCherry) into MPN and HSV-hEfl $\alpha$ -LS1L-EYFP into VMHvl of *Esr1-2A-Cre* male mice (Fig. 1k). Consistent with CTB labeling, PA<sup>Esr1+MPN</sup> and PA<sup>Esr1+VMHvl</sup> cells show largely distinct spatial distribution (Fig. 1l–o) and overlap minimally at the single cell level (PA<sup>Esr1+MPN</sup>/total labeled cells:  $54.3 \pm 0.2\%$ ; PA<sup>Esr1+VMHvl</sup>/total:  $39.6 \pm 0.8\%$ ; Overlap/total:  $6.1 \pm 0.6\%$ ; PA<sup>Esr1+MPN</sup>/PA<sup>Esr1+</sup>:  $21.5 \pm 1.7\%$ ; PA<sup>Esr1+VMHvl</sup>/PA<sup>Esr1+</sup>:  $15.6 \pm 0.6\%$ ; Overlap/PA<sup>Esr1+</sup>:  $2.4 \pm 0.6\%$ ; Predicted Overlap by chance:  $3.4 \pm 0.4\%$ ; *paired t-test* between Predicted Overlap and Observed overlap:  $p = 0.016$ ;  $n = 3$ ; Fig. 1n,o). Additionally, we quantified all retrogradely labeled *Esr1*<sup>+</sup> cells in the amygdala and found that PA contains the largest fraction of labeled *Esr1*<sup>+</sup> cells in both MPN- and VMHvl-targeted animals, pointing to PA as a major source of inputs to the medial hypothalamus (Extended Data Fig. 1).

### Male PA<sup>Esr1+</sup> cells provide monosynaptic excitatory inputs to MPN<sup>Esr1+</sup> and VMHvl<sup>Esr1+</sup> cells

Consistent with previous reports<sup>28,34</sup>, we found that PA consists of mainly excitatory neurons ( $92.3\%$ ,  $n = 2$  mice) using *Vglut1-ires-Cre*  $\times$  Ai6 (a ZsGreen reporter mouse) and *Vgat-ires-Cre*  $\times$  Ai6 male mice (Extended Data Fig. 2a–c). Histological analysis revealed that approximately 50% of PA cells express *Esr1* and over 95% of PA<sup>Esr1+</sup> cells are glutamatergic (Extended Data Fig. 2c).

We next examined whether PA<sup>Esr1+</sup> cells provide direct synaptic inputs to MPN and VMHvl cells, especially the social behavior relevant *Esr1*<sup>+</sup> cells<sup>5,7,29,30,35</sup>. We injected AAV-Efl $\alpha$ -DIO-ChR2-EYFP into the PA and AAV-hSyn-DIO-mCherry into MPN or VMHvl of *Esr1-*

2A-Cre male mice (Fig. 2a). Three weeks later, we performed whole-cell voltage-clamp recordings from mCherry<sup>+</sup> cells in MPN or VMHvl while stimulating PA terminals using 0.5-ms blue light pulses (Fig. 2b). We observed optogenetically-evoked excitatory currents (oEPSCs) as well as inhibitory postsynaptic currents (oIPSCs) in the majority of recorded cells in MPN (53.1%) (Fig. 2b–e). oEPSCs featured a short latency ( $2.24 \pm 0.18$  ms;  $n = 25$  cells) while oIPSCs displayed significantly longer latencies ( $8.58 \pm 1.21$  ms;  $n = 19$  cells), suggesting that the oEPSCs are likely monosynaptic while oIPSCs are polysynaptic (Fig. 2e). Consistent with this hypothesis, bath application of CNQX, an AMPA receptor blocker, abolished both oEPSCs and oIPSCs (Fig. 2f–h).

Similar to the *Esr1*<sup>+</sup> cells in MPN, two thirds of VMHvl<sup>*Esr1*+</sup> cells showed short-latency oEPSCs ( $2.06 \pm 0.20$  ms;  $n = 23$  cells) followed by long-latency oIPSCs ( $10.43 \pm 1.40$  ms;  $n = 20$  cells) upon 0.5 ms light stimulation (Fig. 2i–l). CNQX application abolished both oEPSCs and oIPSCs (Fig. 2m–o). Altogether, these results suggest that PA<sup>*Esr1*+</sup> cells provide direct excitatory and indirect inhibitory inputs to both MPN<sup>*Esr1*+</sup> and VMHvl<sup>*Esr1*+</sup> cells.

### Male PA subregions that project to MPN and VMHvl display differential molecular phenotypes

Given the spatial segregation between PA<sup>MPN</sup> and PA<sup>VMHvl</sup> cells, we wondered whether these two populations also differ molecularly. As a first clue, a higher percentage of PA<sup>MPN</sup> cells overlap with *Esr1* than that of PA<sup>VMHvl</sup> cells (Fig. 1f). To address this question more systematically, we injected red and green retrobeads into MPN and VMHvl of C57BL/6N male mice, respectively, and used later capture microdissection to collect fluorescence-intense PA subregions as well as the adjacent basomedial amygdala posterior part (BMAp), and then performed RNA-sequencing (Fig. 3a). Principal component analysis of RNAseq results revealed that samples from the same PA subregion clustered together and apart from other regions (Fig. 3b). We found 694 genes, including *Esr1*, enriched in PA compared to BMAp (Fig. 3c, Supplementary Table 2). Additionally, 172 genes were found at a higher level (fold change > 1.5) in the MPN-projecting subregion of PA compared to the VMHvl-projecting subregion, and 215 genes showed the opposite pattern (Fig. 3e, Supplementary Table 2). Then, we performed *in situ* hybridization to visualize mRNA expression of several candidate genes enriched in PA<sup>36</sup>. Consistent with the RNAseq data, *Pde11a*, *Prokr2* and *Zic2* were expressed at high levels in the entire PA but not in the neighboring BMAp (Fig. 3d). *Chrna7*, *Npy2r* and *Nnat* predominantly localized to the MPN-projecting dorsomedial part of PA whereas *Etv1*, *Calb2* and *Dlk1* were largely confined to the VMHvl-projecting ventrolateral part of PA (Fig. 3f). Double *in situ* hybridization of *Chrna7* and *Dlk1* revealed their largely non-overlapping expression in PA (*Dlk1*<sup>+</sup>:  $27.5 \pm 2.5$  cells/section; *Chrna7*<sup>+</sup>:  $71.8 \pm 2.8$  cells/section; *Chrna7*<sup>+</sup>*Dlk1*<sup>+</sup>:  $2.0 \pm 0.3$  cells/section;  $n = 4$  sections from 2 animals). Lastly, we combined retrograde tracing and *in situ* hybridization and confirmed that over 90% of PA<sup>MPN</sup> cells expressed *Chrna7* whereas over 80% of PA<sup>VMHvl</sup> cells expressed *Dlk1* (Fig. 3g–i). Altogether, these data suggest that two largely distinct PA subpopulations with different gene expression and hypothalamic projection patterns exist in male mice.

## PA<sup>Esr1+MPN</sup> and PA<sup>Esr1+VMHvl</sup> cells respond differentially during male sexual behaviors and aggression

To understand whether *Esr1* marks the social behavior relevant population in PA, we performed double staining of c-Fos and *Esr1* in animals that experienced mating and fighting. 74% and 67% of mating and fighting induced c-Fos<sup>+</sup> cells contained *Esr1*, respectively, significantly higher than chance (~50%) (Extended Data Fig. 3a–e). Additionally, c-Fos<sup>+</sup> cells induced by male mating and fighting distributed to different subregions of PA: while mating-induced c-Fos was concentrated in the anterior half of PA, fighting-induced c-Fos distributed evenly along the anterior-posterior axis of PA (Extended Data Fig. 3f). As mating and fighting induced c-Fos expression patterns matched with MPN and VMHvl retrograde labeling patterns in the PA, respectively, we next investigated the potential differential responses of PA<sup>Esr1+MPN</sup> and PA<sup>Esr1+VMHvl</sup> cells in male sexual and aggressive behaviors.

We performed fiber photometric recording in *Esr1-2A-Cre* male mice by injecting HSV-hEfl $\alpha$ -LSL-GCaMP6f into the MPN or VMHvl and implanted an optic fiber above PA (Fig. 4a, b, Extended Data Fig. 4)<sup>7,37,38</sup>. Histological analysis revealed that majority of GCaMP6f<sup>+</sup> cells overlapped with *Esr1* (93.5  $\pm$  1.0% cells,  $n = 3$  animals; Fig. 4c). Consistent with the fact that a higher percentage of PA<sup>MPN</sup> cells express *Esr1*, we observed a higher number of GCaMP6f<sup>+</sup> cells in PA in animals with virus injected into MPN than in VMHvl (PA<sup>Esr1+MPN</sup>: 310  $\pm$  31 cells/animal; PA<sup>Esr1+VMHvl</sup>: 171  $\pm$  13 cells/animal,  $n = 5$  animals each).

We found that PA<sup>Esr1+MPN</sup> and PA<sup>Esr1+VMHvl</sup> cells showed complementary response patterns during male-male and male-female encounters (Fig. 4d–z). PA<sup>Esr1+MPN</sup> neurons showed a greater increase in Ca<sup>2+</sup> upon female introduction than male introduction as well as higher responses during female investigation than male investigation (Fig. 4f–i, z). By contrast, PA<sup>Esr1+VMHvl</sup> cells showed higher responses to males than females, during both entrance and investigation (Fig. 4q–t, z). Complementary responses in PA<sup>Esr1+MPN</sup> and PA<sup>Esr1+VMHvl</sup> cells persisted throughout the consummatory phase of social behaviors: PA<sup>Esr1+MPN</sup> cells showed stronger signals during male mating than attacking, while PA<sup>Esr1+VMHvl</sup> cells showed significantly higher responses during attacking than mating (Fig. 4j–n, u–z). We noticed that Ca<sup>2+</sup> increases of PA<sup>Esr1+MPN</sup> cells often preceded mounting onset, which was defined as the moment when the male first clasped its forelimbs around the female's body (Fig. 4j). To understand the precise temporal relationship between mounting initiation and PA<sup>Esr1+MPN</sup> cell activity, we tracked the position of the male and identified a subset of trials when the male initiated mounting after a short period (> 2 s) of quiescence. We reasoned that the onset of locomotion in those trials likely indicates the beginning of a mounting attempt. In those trials, we found that Ca<sup>2+</sup> increased simultaneously or slightly before elevations in velocity (Extended Data Fig. 5a–e). Importantly, increases in PA<sup>Esr1+MPN</sup> Ca<sup>2+</sup> do not simply reflect movement initiation as no increases were observed when recorded males initiated movements without subsequent mounting attempts (Extended Data Fig. 5a–e). PA<sup>Esr1+MPN</sup> cells continued to increase activity as sexual behaviors advanced (Fig. 4j–m, z). In contrast, PA<sup>Esr1+VMHvl</sup> cells showed the highest response during fighting against male intruders (0.18  $\pm$  0.03,  $n = 5$  animals) and only increased activity

moderately during the advanced stages of sexual behaviors (Fig. 4u–z). In contrast to the  $PA^{Esr1+MPN}$  cells,  $PA^{Esr1+VMHvl}$  cells showed no consistent increase in activity when the male initiated mounting (Extended Data Fig. 5f–j). Investigation of a plastic object elicited no detectable change in the activity of either  $PA^{Esr1+MPN}$  or  $PA^{Esr1+VMHvl}$  cells (Fig. 4z, Extended Data Fig. 6a–d). In three control animals that expressed GFP in  $PA^{Esr1+}$  cells, we observed little change in fluorescence during any social behaviors (Extended Data Fig. 6e–q). Altogether, these data show that male PA preferentially sends mating-related signals to MPN and aggression-related signals to VMHvl.

### Inhibitions of male $PA^{Esr1+MPN}$ and $PA^{Esr1+VMHvl}$ cells cause largely distinct deficits in social behaviors

Next, we investigated whether  $PA^{Esr1+MPN}$  and  $PA^{Esr1+VMHvl}$  cells are necessary for male sexual and aggressive behaviors. We injected a retrograde HSV expressing *Cre*-dependent *Flippase (Flp)* into either MPN or VMHvl bilaterally and AAV-Ef1 $\alpha$ -fDIO-hM4Di-mCherry<sup>39</sup> into the PA bilaterally of *Esr1-2A-Cre* male mice (Fig. 5a, b). As expected, the vast majority of hM4Di-mCherry expressing cells were positive for *Esr1* ( $86.9 \pm 0.6\%$ ,  $n = 3$  animals; Fig. 5c) and located in PA ( $88.0 \pm 2.4\%$  in  $PA^{Esr1+MPN}$  and  $91.3 \pm 3.8\%$  in  $PA^{Esr1+VMHvl}$ ,  $n = 8$  animals each; Extended Data Fig. 4b).

Three weeks after virus injection, we screened for animals that showed consistent sexual and aggressive behaviors before injecting CNO and saline on separate days. In males expressing hM4Di in  $PA^{Esr1+MPN}$  cells, CNO nearly abolished sexual behaviors but did not affect aggressive behaviors (Fig. 5d–m). On saline-injected day, all tested males showed sexual behaviors towards a receptive female and achieved deep-thrust within the 10-minutes test period. Strikingly, on CNO-injected days, 5/8 males did not attempt to mount and none achieved deep-thrust (Fig. 5e–j). In contrast, aggressive behaviors, including attack duration and latency to attack, was not affected (Fig. 5l, m). Investigatory behaviors towards female increased, possibly as a result of the decrease in sexual behaviors, while male investigation duration remained unchanged (Fig. 5d, k). In a separate experiment, we examined changes in male sexual behaviors after hM4Di-mediated inactivation of an unselected population of  $PA^{Esr1+}$  cells and observed similarly striking impairments in sexual behaviors (Extended Data Fig. 7).

Inactivating the male  $PA^{Esr1+VMHvl}$  cells caused different behavioral deficits. While CNO injection did not reduce mounting attempts or shallow-thrust, it decreased the duration of deep-thrust and increased its latency (Fig. 5o–t), consistent with a reported role of VMHvl in intromission<sup>13</sup>. Furthermore,  $PA^{Esr1+VMHvl}$  inactivation caused a significant decrease in aggression, as indicated by a significant diminution in attack duration (Fig. 5v, w). Investigations towards males and females were unchanged after  $PA^{Esr1+VMHvl}$  inactivation (Fig. 5n, u). Altogether,  $PA^{Esr1+MPN}$  cells are indispensable for all aspects of male sexual behaviors while  $PA^{Esr1+VMHvl}$  cells mainly mediate male aggression but also play a minor role in advanced stages of sexual behaviors.

## Pharmacogenetic activations of male PA<sup>Esr1+MPN</sup> and PA<sup>Esr1+VMHvl</sup> neurons promote sexual and aggressive behaviors respectively

To test whether PA<sup>Esr1+MPN</sup> and PA<sup>Esr1+VMHvl</sup> cells are sufficient to drive male sexual and aggressive behaviors respectively, we bilaterally injected HSV-hEfl $\alpha$ -LS1L-*Flp* into either MPN or VMHvl and AAV-Ef1 $\alpha$ -fDIO-hM3Dq-mCherry into bilateral PA in *Esr1-2A-Cre* male mice (Fig. 6a, b). Histological analysis revealed that vast majority of hM3Dq-mCherry expressing cells were positive for *Esr1* ( $89.1 \pm 7.0\%$ ,  $n = 3$  animals; Fig. 6c) and confined in PA ( $88.2 \pm 2.8\%$  in PA<sup>Esr1+MPN</sup>,  $n = 8$  and  $94.0 \pm 2.0\%$  in PA<sup>Esr1+VMHvl</sup>,  $n = 6$  animals; Extended Data Fig. 4c). All tested males were naïve to minimize spontaneous aggression and sexual behaviors.

During testing, we sequentially introduced a non-receptive adult female and a group-housed nonaggressive male into the home cage of the test male mice. In males expressing hM3Dq in PA<sup>Esr1+MPN</sup> cells, i. p. injection of low dose of CNO (0.1 mg/kg) promoted female-directed sexual behaviors without altering aggressive or investigatory behaviors towards either males or females (Fig. 6d–q). On saline-injected day, 4/8 males showed mounting attempts and only 2/8 achieved brief shallow thrust. In contrast, after CNO injection, all males attempted to mount, often repeatedly, and all achieved shallow thrust despite the uncooperative behaviors of the non-receptive females (Fig. 6e–h). Interestingly, when 0.5 mg/kg CNO was administered, which induces a higher level of neural activation than 0.1 mg/kg CNO<sup>40</sup>, we observed a mixture of sexual and aggressive behaviors towards females: all males showed sexual behaviors and half of those animals also attacked females after several mounting attempts (Extended Data Fig. 8a–g). Importantly, the aggressive behavior appears to be specifically directed towards females as male-directed aggression did not change, suggesting that PA<sup>Esr1+MPN</sup> cells do not promote natural inter-male aggression (Extended Data Fig. 8a, h–m).

By contrast, activating PA<sup>Esr1+VMHvl</sup> cells did not affect sexual or investigatory behaviors towards either males or females at either CNO concentration (Fig. 6r–ee and Extended Data Fig. 8n–z). However, administering CNO but not saline promoted aggression in a dose-dependent manner. While only 2 out of 8 males attacked males after saline injection, 5 out of 8 attacked males and 2 attacked females with 0.1 mg/kg CNO (Extended Data Fig. 8s, t, y, z). At 0.5 mg/kg CNO, all animals attacked males and 6/8 also attacked females (Fig. 6w, x, dd, ee), strongly suggesting that PA<sup>Esr1+VMHvl</sup> cells promote aggressive behaviors.

We also activated PA<sup>Esr1+VMHvl</sup> and PA<sup>Esr1+MPN</sup> cells optogenetically (20 Hz, 20 ms, 0.5–7.5 mW). While activation of PA<sup>Esr1+VMHvl</sup> cells elicited stimulation-locked attack, we did not observe any increase in sexual behaviors upon optogenetic activation of PA<sup>Esr1+MPN</sup> cells (Extended Data Fig. 9). In fact, these animals showed very little sexual behaviors during the entire testing period, suggesting that strong and synchronous exogenous stimulation of PA<sup>Esr1+MPN</sup> cells is insufficient to promote sexual behaviors. Taken together, activation of PA<sup>Esr1+VMHvl</sup> neurons can elicit aggression while enhancing the natural responses of PA<sup>Esr1+MPN</sup> cells promotes male sexual behaviors towards females.

### Connectivity of male PA<sup>Esr1+MPN</sup> and PA<sup>Esr1+VMHvl</sup> neurons

To achieve a comprehensive understanding of the connectivity of PA<sup>Esr1+MPN</sup> and PA<sup>Esr1+VMHvl</sup> cells, we injected retrograde HSV-hEfl $\alpha$ -LS1L-*Flp* into either MPN or VMHvl and AAV-hSyn-Con/Fon-EYFP in the PA of *Esr1-2A-Cre* male mice (Fig. 7a, b). As expected, we found that PA<sup>Esr1+MPN</sup> neurons project densely to MPN while PA<sup>Esr1+VMHvl</sup> neurons project strongly to VMHvl (Fig. 7c–e). PA<sup>Esr1+MPN</sup> cells largely spare VMHvl while some fibers in MPN were observed from PA<sup>Esr1+VMHvl</sup> cells, indicating that PA<sup>Esr1+VMHvl</sup> may influence the MPN activity to some extent. This difference may also be because PA axons route through stria termanlis to hypothalamus and thus VMHvl-targeting fibers need to course through MPN while MPN-targeting axons do not pass VMHvl<sup>26</sup> (Fig. 7c–e). Additionally, PA<sup>Esr1+MPN</sup> and PA<sup>Esr1+VMHvl</sup> neurons send collaterals to several regions inside and outside of the hypothalamus, but with clear distinctions. Within the hypothalamus, the other major target of PA<sup>Esr1+MPN</sup> neurons is the anteroventral periventricular nucleus (AVPV) whereas ventral premammillary nucleus (PMv) is the other main region receiving inputs from PA<sup>Esr1+VMHvl</sup> neurons (Fig. 7c). Outside of the hypothalamus, PA<sup>Esr1+MPN</sup> but not PA<sup>Esr1+VMHvl</sup> cells project to the lateral septum ventral part (LSv) (Fig. 7c–e). Finally, both PA<sup>Esr1+MPN</sup> and PA<sup>Esr1+VMHvl</sup> cells project densely to the MeApd and BNSTpr, and moderately to the ventral subiculum (vSub), suggesting possible convergence of information in those areas. Altogether, the anterior biased PA<sup>Esr1+MPN</sup> neurons show an anterior-biased projection pattern (AVPV and MPN) whereas the PA<sup>Esr1+VMHvl</sup> neurons show a posterior-biased projection pattern (VMHvl and PMv).

We next used projection-specific monosynaptic rabies tracing to map inputs to PA<sup>Esr1+MPN</sup> and PA<sup>Esr1+VMHvl</sup> cells<sup>41</sup>. We injected HSV-hEfl $\alpha$ -LS1L-*Flp* into either MPN or VMHvl, and AAVs expressing *Flp*-dependent TVA receptors and a rabies glycoprotein into the PA of *Esr1-2A-Cre* male mice. After 2 weeks, EnvA-pseudotyped, glycoprotein-deleted rabies virus (EnvA-RV G-eGFP) was injected into PA (Fig. 7f). Seven days later, we examined inputs (eGFP<sup>+</sup> cells) to PA<sup>Esr1+MPN</sup> and PA<sup>Esr1+VMHvl</sup> starter cells (eGFP<sup>+</sup>mCherry<sup>+</sup> cells) across the entire brain (Fig. 7g–l). Hippocampus represents the largest input to both PA<sup>Esr1+MPN</sup> and PA<sup>Esr1+VMHvl</sup> cells. Approximately half of all retrogradely labeled cells, regardless of the PA starter cell population, were located in hippocampus, including approximately 30% in CA1 and 20% in vSub (Fig. 7h, j, l). Several other regions including medial septum (MS), paraventricular thalamus (PVT), posterolateral (CoApl) and posteromedial part of cortical amygdala (CoApm) and BMAp also provide moderate inputs to both PA<sup>Esr1+MPN</sup> and PA<sup>Esr1+VMHvl</sup> cells. Interestingly, PMv and MeApd, two regions that are known to project to PA appear to target the PA<sup>Esr1+MPN</sup> subpopulation preferentially<sup>26,42</sup> whereas PA<sup>Esr1+VMHvl</sup> cells receive relatively strong inputs from regions processing volatile olfactory information, including piriform cortex (Pir) and piriform-amygdalar area (PAA) (Fig. 7h, j, l)<sup>43</sup>. Altogether, PA<sup>Esr1+MPN</sup> and PA<sup>Esr1+VMHvl</sup> are both well positioned to integrate olfactory, contextual, experiential and emotional state related information and serves as an important player in the male sexual and aggressive circuit respectively.

## Discussion

In this study, we identified PA as a key node in both the aggression and mating circuits in male mice. Specifically, we found two largely distinct PA subpopulations that project to MPN and VMHvl and each serves important social functions in male mice. Among PA cells that project to MPN or VMHvl, less than 10% of cells project to both regions. PA<sup>Esr1+MPN</sup> neurons gradually increase activity as sexual behaviors advance and are necessary and sufficient for the behaviors. By contrast, PA<sup>Esr1+VMHvl</sup> cells play only a minor role in sexual behaviors, and are excited mainly during inter-male aggression and promote attack. Cell-type specific tracing revealed that PA<sup>Esr1+MPN</sup> and PA<sup>Esr1+VMHvl</sup> cells receive rich inputs from hippocampal regions and project densely to medial hypothalamus as well as brain regions along the vomeronasal pathway.

### PA neurons play important roles in male sexual and aggressive behaviors

Nearly three decades ago, Canteras and colleagues performed classical anterograde tracing from PA, revealing its dense projection to the medial hypothalamus, and accordingly proposed a role for PA in social behaviors<sup>26</sup>. Despite this early insight, the functional role of PA in male social behaviors has not been examined for decades<sup>44</sup>. Recently, Zha et.al. reported that vesicular glutamate transporter 1 (Vglut1) expressing cells in the PA that project to the VMHvl can bi-directionally modulates male aggression<sup>44</sup>. This result is largely consistent with our findings showing a key role of PA<sup>Esr1+VMHvl</sup> cells in male aggression. However, PA<sup>Esr1+VMHvl</sup> cells are likely to be more aggression-specific than the PA<sup>Vglut1+VMHvl</sup> cells as PA<sup>Esr1+VMHvl</sup> but not PA<sup>Vglut1+VMHvl</sup> cells showed a consistent Ca<sup>2+</sup> increase during male investigation and attack<sup>44</sup>. Indeed, while over 95% of Esr1+ cells express Vglut1, less than half of the Vglut1+ cells express Esr1 (Extended Data Fig. 2).

Our results further demonstrate an indispensable role of Esr1+ neurons in PA in male sexual behaviors: inhibiting PA<sup>Esr1+</sup> cells or PA<sup>Esr1+MPN</sup> cells abolishes virtually all aspects of sexual behaviors. The central role of the PA in sexual behavior is particularly striking considering the relatively inconsistent behavioral deficit caused by inhibiting other major upstream regions of MPN, including MeA, BNSTpr and VMHvl. Killing the aromatase-expressing cells or acutely inhibiting GABAergic cells (the major population) within MeA does not decrease sexual behaviors in male mice<sup>14,17</sup>. Lesioning BNST causes only minor impairments in sexual behaviors such as increased latency to ejaculate<sup>45,46</sup> although a recent study showed that inactivation or ablation of aromatase neurons in BNSTpr reduced intromission and ejaculation<sup>23</sup>. Killing VMHvl progesterone (PR) expressing cells slightly decrease the number of intromission<sup>8</sup>. In contrast, inactivation of PA<sup>Esr1+MPN</sup> cells compromised the entire sequence of the male sexual behaviors - from mounting initiation to ejaculation.

In contrast to clear behavior changes elicited by optogenetic activation of PA<sup>Esr1+VMHvl</sup> cells, optogenetic stimulation of PA<sup>Esr1+MPN</sup> cells failed to elicit sexual behaviors. This could be because mating is a multi-stage sequential process and MPN contains cells with diverse response patterns during sexual behaviors: some MPN cells are excited during pursuit of females and mounting initiation but inhibited during intromission while others are activated only during advanced stages of sexual behaviors<sup>47</sup>. Non selective, synchronous

activation of PA<sup>Esr1+MPN</sup> afferents likely recruit MPN cells with diverse functions and thus fail to drive a coherent behavioral motor program. Additionally, unlike VMHvl cells which are mainly glutamatergic, MPN cells are primarily GABAergic and form extensive local synapses<sup>48</sup>. Thus, activation of functionally diverse MPN cells by PA may lead to a general suppression of activity and consequently a lack of sexual behaviors altogether. Unlike optogenetic activation that directly evokes action potentials, hM3Dq activation increases the excitability of cells by engaging endogenous Gq signaling. Importantly, hM3Dq mediated neural activation is dependent on ligand concentration. A previous study using mice expressing hM3Dq in the cortical pyramidal cells found that 0.1 mg/kg CNO induced an increase in locomotion while 0.5 mg/kg CNO elicited seizures<sup>40</sup>, suggesting that CNO can be titrated to elevate neural activity within a physiological range. It is therefore likely that the endogenous synaptically-driven spiking pattern of PA neurons, which in turn contribute to the diverse response patterns of MPN cells, is essential for generating complex behavioral sequences like mating.

### PA enriched genes and their relevance to social behaviors

Mating- and aggression-related PA subregions show clear differences in gene expression patterns. Differentially expressed genes include transcription factors (*Etv1*, *Zic2*), G-protein coupled receptors (*Npy2r*, *Prokr2*), ion channels (*Chrna7*), calcium binding proteins (*Calb2*) amongst others. One of the PA enriched genes, *Zic2*, has been implicated previously in aggression: mice with hypomorphic mutations in *Zic2* decreased inter-male aggression and social dominance<sup>49</sup>. Interestingly, the authors also noted a high abundance of *Zic2* in PA and a decreased cell density in the area in mutant mice. Furthermore, while wild-type mice show strong acetylcholine esterase (AChE) staining in PA, AChE levels are low in mutant animals<sup>49</sup>. The strong AChE staining in PA is consistent with our finding that *Chrna7* expresses highly in the PA. Our retrograde tracing revealed that PA receives a moderate input from MS, a region containing abundant cholinergic cells, suggesting PA as a potential site for cholinergic modulation of aggression<sup>50</sup>.

### Sexually dimorphic PA

What is the function of PA in females? Anatomical studies in rodents revealed that PA exists in both males and females with comparable volume, morphology and cell density<sup>28</sup>. However, several lines of evidences suggest that PA is likely to play sexually dimorphic roles in social behaviors. First, MPN serves differential functions between males and females. While MPN is the central region for male sexual behavior, its primary function in females is to mediate maternal behaviors<sup>1–5,29</sup>. Second, VMHvl function is sexually dimorphic. While VMHvl is key to male aggression and only plays a minor role in male sexual behaviors, it is indispensable for both female sexual behaviors and aggression<sup>6,8,30</sup>. In females, VMHvl appears to contain a molecularly distinct compartment specialized for female sexual behaviors that is absent in males<sup>30</sup>. Third, PA shows sexually dimorphic projection pattern. While both male and female PA cells project to MPN, VMHvl, BNSTpr and MeApd, female PA appears to lack a strong projection to AVPV<sup>28</sup>. Taken together, we speculate that female PA could be relevant for various social behaviors, including maternal, sexual and aggressive behaviors. The organizations of those behavior-relevant populations and their downstream circuits are likely to differ from those in males. Future studies

focusing on the PA in females will help elucidate the sexual dimorphism of social behavior circuits.

### **The placement of PA in the social behavior circuits in males**

In 2000, Larry Swanson proposed a basic wiring diagram for controlling motivated behaviors based on extensive developmental and neuroanatomical evidence<sup>34</sup>. In his model, forebrain exerts “top-down” voluntary control on various motivated behaviors through a set of triple descending projections to the “behavioral control column” in the upper brainstem<sup>34</sup>. The rostral part of the behavior control column is for ingestive and social behaviors, and contains several hypothalamic nuclei, including MPN and VMHvl. The caudal part of the column is for general exploratory and foraging behaviors and contains mammillary nucleus, substantia nigra (SNr) and ventral tegmental area. In his view, the overall pattern of motivational behavior circuitry originating in the cortical map, with its regionalization into functionally distinct areas, and then involving sequentially the striatum and pallidum, followed by the brainstem. The cortical projection is primarily glutamatergic whereas the striatal and pallidal projections are primarily GABAergic. A familiar example of the triple projection is the isocortical-dorsal striatopallidal system in which (1) cortical regions send direct glutamatergic projections to the SNr and collateral and topographic projections to dorsal striatum; (2) dorsal striatum sends GABAergic projection to the SNr with a collateral projection to the pallidum; (3) pallidum then sends GABAergic projection to the SNr with a collateral to the thalamus, which in turn projects to cortex (Extended Data Fig. 10). Importantly, in this grand scheme, each and all of the anatomical structures in the cerebral hemisphere belong to either prototypical cortex, striatum or pallidum.

According to this view, we propose that PA along with the heavily interconnected vSub constitute the “social cortex” and mediate top-down regulation of the hypothalamic behavior control column. Similar to the classical isocortical-dorsal striatopallidal system, PA/vSub, MeA and BNST provide a triple descending projection to the column (Extended Data Figure 10). First, PA/vSub (cortex) sends excitatory projection directly to the column (MPN and VMHvl) as well as collaterals to the MeA (rostrocaudal striatum)<sup>34</sup>. MeA then sends inhibitory projection to the same part of the behavior column (MPN and VMHvl) as well as collaterals to the BNST (rostrocaudal pallidum). Lastly, BNST provides disinhibitory projection to the column. In this model, PA/vSub occupies a similar position in social behavior circuit as the motor cortex in voluntary motor circuit and determines the timing of the behavior initiation. Indeed, PA cells increase activity when the animal makes the first move towards the female to initiate mount. Suppressing PA activation blocks the initiation of sexual behaviors altogether.

The discovery of PA as a key node for social behaviors supports the existence of a universal diagram underlying cortical control of movement. PA is potentially a specialized “cortex” to control a set of stereotypical movements constituting innate social behaviors. This study offers a novel framework for understanding how social behaviors are organized and initiated at the circuit level and opens new avenues for studying the neural generation of innate behaviors.

## Methods

### Mice

All procedures were approved by NYULMC IACUC in compliance with the NIH guidelines for Care and Use of Laboratory Animals. Adult mice 12–38 weeks of age were used for all studies. Mice were housed in 18–23°C with 40–60 % humidity under a 12 h light-dark cycle (10 p.m. to 10 a.m. light), with food and water available *ad libitum*. Animals used for CTB retrograde tracing and RNA-Seq experiments were 14–16 week old wild-type C57BL/6N male purchased from Charles River. Male *Esr1-2A-Cre* (14–38 weeks, Jackson Stock No. 017911), male *Vgat-ires-Cre* × Ai6 (12–16 weeks, Jackson stock No. 016962 and 007906)<sup>52</sup>, male *Vglut1-ires-Cre* × Ai6 (12–16 weeks, Jackson stock No. 023527 and 007906)<sup>53</sup> were used for functional, recording and histological experiments. Stimulus animals were adult C57BL/6N female and male or BALB/c male mice (> 8 weeks) purchased from Charles River. Stimulus animals were group housed. After surgery, all test animals were singly housed. All the experiments were performed during the dark cycle of the animals.

### Viruses

AAV2-CAG-FLEX-GFP, AAV2-hSyn-DIO-mCherry, AAV1-Ef1 $\alpha$ -DIO-hM4Di-mCherry, AAV5-hSyn-Con/Fon-EYFP, AAV2-Ef1 $\alpha$ -DIO-ChR2-EYFP, AAVDJ-Ef1 $\alpha$ -fDIO-EYFP and AAVDJ-hSyn-Con/Fon-hChR2(H134R)-EYFP were purchased from the University of North Carolina vector core. AAV5-CAG-FLEX(FRT)-TC and AAV8-CAG-FLEX(FRT)-G were purchased from the vector core of Stanford University. AAVDJ-Ef1 $\alpha$ -fDIO-hM4Di-mCherry and AAVDJ-Ef1 $\alpha$ -fDIO-hM3Dq-mCherry were made in Byungkook Lim lab. HSV-hEf1 $\alpha$ -LS1L-EYFP, HSV-hEf1 $\alpha$ -LS1L-*Ffp*, HSV-hEf1 $\alpha$ -LS1L-mCherry and HSV-hEf1 $\alpha$ -LSL-GCaMP6f was purchased from Massachusetts General Hospital Neuroscience Center vector core. EnvA-G-Deleted Rabies-EGFP was purchased from Salk Institute vector core. All AAV titers ranged from  $3.00 \times 10^{12}$  to  $4.30 \times 10^{13}$  genomic copies/mL. All HSV titers were  $1.00 \times 10^9$  genomic copies/mL. Rabies virus titers were  $> 3.00 \times 10^7$  transforming units/mL.

### Stereotactic surgery

Mice (12–20 weeks) were anesthetized with isoflurane (1–1.5%) and placed in a stereotaxic apparatus (Kopf Instruments Model 1900). Viruses and tracers were delivered into the targeted brain regions as described previously<sup>29</sup>. All animals included in the final analysis have correct injection sites as verified by histology.

For single retrograde tracing experiments, 20 nL of Alexa555 conjugated CTB (Thermo Fisher, C22843) was injected into the unilateral MPN (AP: –0.31 mm, ML:  $\pm 0.31$  mm, DV: –4.95 mm) or VMHv1 (AP: –1.45 mm, ML:  $\pm 0.655$  mm, DV: –5.655 mm). 3/4 and 3/6 animals that showed correct unilateral targeting in MPN and VMHv1, respectively, were included in the final analysis.

For dual retrograde CTB tracing experiments, 20 nL of Alexa555-CTB and Alexa647-CTB (Thermo Fisher, C22843 and C34778) was injected into the MPN and VMHv1, respectively.

Brains were harvested 10 days later. 3/5 animals with correct targeting in both MPN and VMHvl were included.

For microdissection of distinct subregions in the PA, 30 nL of Red and Green retrobeads (Lumafuor Item, R170, G170) were injected into unilateral MPN and VMHvl, respectively. Brains were harvested 7 days later. 3/5 animals with correct targeting in both MPN and VMHvl were included in the final analysis.

For dual-retrograde tracing, HSV-hEfl $\alpha$ -LS1L-mCherry and HSV-hEfl $\alpha$ -LS1L-EYFP were injected into ipsilateral MPN and VMHvl, respectively. Brains were harvested two weeks later. 3/7 animals that showed correct unilateral targeting in both MPN and VMHvl were included in the final analysis.

For investigating the outputs of PA<sup>Esr1+MPN</sup> and PA<sup>Esr1+VMHvl</sup> projectors, 100 nL (130 nL) of HSV- hEfl $\alpha$ -LS1L-*Flp* was injected into the MPN (VMHvl) and simultaneously 100 nL of AAV5-hSyn-Con/Fon-EYFP was injected into the ipsilateral PA (AP: -2.30 mm, ML:  $\pm$ 2.40 mm, DV: -4.80 mm). Brains were harvested two weeks later. 3/5 animals that showed correct unilateral targeting in the MPN and correct virus expression in the PA and 3/5 animals that showed correct unilateral targeting in the VMHvl and correct unilateral virus expression in the PA were included in the final analysis.

For investigating the inputs of PA<sup>Esr1+MPN</sup> and PA<sup>Esr1+VMHvl</sup> cells, 100 nL (130 nL) of HSV- hEfl $\alpha$ -LS1L-*Flp* was injected into the MPN (VMHvl) and simultaneously 180 nL 1:1 AAV5-CAG-FLEX(FRT)-TC and AAV8-CAG-FLEX(FRT)-G were injected into the ipsilateral PA. After two weeks, 600 nL EnvA-G-Deleted Rabies-eGFP was injected into the PA of the same side. One week later, the brain was harvested for histological analysis. 3/5 animals that showed correct unilateral targeting in the MPN and correct virus expression in the PA and 3/6 animals that showed correct unilateral targeting in the VMHvl and correct virus expression in the PA were included in the final analysis.

For the slice recording experiment, 100 nL AAV2-Ef1 $\alpha$ -DIO-ChR2-EYFP was injected into the PA and simultaneously 100 nL AAV2-hSyn-DIO-mCherry was injected into the MPN or VMHvl. The brains were used for recording three weeks later. 10/12 animals that showed correct unilateral targeting in MPN, VMHvl and PA were included in the final analysis.

For fiber photometric recording of the PA<sup>Esr1+MPN</sup> (PA<sup>Esr1+VMHvl</sup>) population, 100 nL (130 nL) HSV-hEfl $\alpha$ -LSL-GCaMP6f was injected into MPN (VMHvl). Control animals were injected with 100 nL of AAV2-CAG-FLEX-GFP unilaterally injected into the PA. Then, a custom made optic fiber assembly (Thorlabs, FR400URT, CF440) was inserted  $\sim$ 150  $\mu$ m above the dorsal boundary of the PA and secured using dental cement (C&B Metabond, S380). All recordings start two weeks after virus injection. 7/8 animals that showed correct unilateral targeting in the MPN and correct expression of GCaMP6f and fiber placement in the PA were included in the final analysis. 5/8 animals that showed correct unilateral targeting in the VMHvl and correct GCaMP6f expression and fiber placement in the PA were included in the final analysis.

For pharmacogenetic inhibition of PA<sup>Esr1+</sup> cells, 100 nL of AAV1-hSyn-DIO-hM4Di-mCherry was injected bilaterally into the PA. Control animals were injected with 100 nL of AAV2-hSyn-DIO-mCherry into the PA bilaterally. 5/9 test animals that showed correct bilateral targeting of PA were included in the final analysis.

For pharmacogenetic inhibition of PA<sup>Esr1+MPN</sup> or PA<sup>Esr1+VMHvl</sup>, 100 nL (130 nL) of HSV-hEfl $\alpha$ -LS1L-*Flp* was injected into the MPN (VMHvl) and simultaneously 100 nL of AAVDJ-Efl $\alpha$ -fDIO-hM4Di-mCherry was injected into the PA bilaterally. Control animals were injected with 100 nL (130 nL) of HSV-hEfl $\alpha$ -LS1L-*Flp* into the MPN (VMHvl) bilaterally and 100 nL of AAVDJ-Efl $\alpha$ -fDIO-EYFP into the PA bilaterally. 8/10 test animals that showed correct bilateral targeting in the MPN and correct bilateral virus expression in the PA were included in the final analysis. 8/10 test animals that showed correct bilateral targeting in the VMHvl and correct bilateral virus expression in the PA were included.

For pharmacogenetic activation of PA<sup>Esr1+MPN</sup> or PA<sup>Esr1+VMHvl</sup> cells, 100 nL (130 nL) of HSV-hEfl $\alpha$ -LS1L-*Flp* was injected into the MPN (VMHvl) and simultaneously 120 nL of AAVDJ-Efl $\alpha$ -fDIO-hM3Dq-mCherry was injected into the PA bilaterally. Control animals were injected with 100 nL (130 nL) of HSV-hEfl $\alpha$ -LS1L-*Flp* into the MPN (VMHvl) bilaterally and 100 nL of AAVDJ-Efl $\alpha$ -fDIO-EYFP into the PA bilaterally. 8/11 test animals that showed correct bilateral targeting in the MPN and correct bilateral virus expression and fiber placement in the PA were included in the final analysis. 8/14 test animals that showed correct bilateral targeting in the VMHvl and correct bilateral virus expression and fiber placement in the PA were included in the final analysis.

For optogenetic stimulation of PA<sup>Esr1+MPN</sup> or PA<sup>Esr1+VMHvl</sup> cells, 100 nL (130 nL) of HSV-LS1L-*Flp* was bilaterally injected into the MPN (VMHvl) and simultaneously 200 nL of AAVDJ-hSyn-Con/Fon-hChR2(H134R)-EYFP was injected into the PA bilaterally. Control animals were injected with 130 nL of HSV-hEfl $\alpha$ -LS1L-*Flp* bilaterally injected into the VMHvl and simultaneously 150 nL of AAV5-hSyn-Con/Fon-EYFP into the PA bilaterally. Then, a 200- $\mu$ m optic fiber assembly (Thorlabs, FT200EMT, CFLC230) was implanted 200  $\mu$ m above each side of the PA during the same surgery. 5/10 test animals that showed correct bilateral targeting in the MPN, correct bilateral expression of ChR2-EYFP in the PA and correct bilateral fiber placements in the PA were included in the final analysis. 5/16 test animals that showed correct bilateral targeting in the VMHvl, correct bilateral expression of ChR2-EYFP in the PA (> 100 positive cells in all sections) and bilateral fiber placements in the PA were included in the final analysis.

## Immunohistochemistry

Immunofluorescence staining proceeded as previously described<sup>29,30</sup>. Briefly, mice were perfused transcardially with 1  $\times$  PBS followed by 4% paraformaldehyde (PFA) in 0.1 M PBS. Brains were extracted, post-fixed in 4% PFA for 2–3 hours at 4°C followed by 48 hours in 15% sucrose, embedded in OCT mounting medium, frozen on dry ice, cut to 50  $\mu$ m thick sections using a cryostat (Leica Biosystems) and collected in PBS using 12 well plate. For antibody staining, brain sections were washed with PBS three times and blocked in PBS-T (0.3% Triton X-100 in 1  $\times$  PBS) with 10% normal donkey serum for 1 hour at room

temperature. Sections were then incubated in primary antibody diluted in blocking solution at 4°C for 24–72 hours. We stained for Esr1 (rabbit anti-Esr1; 1:1000; Santa Cruz, sc-542, Lot #F1715), Fos (goat anti-Fos; 1:1000; Santa Cruz, sc52-g), or GFP (rabbit anti-GFP; 1:1000; Thermo Fisher, A11122)<sup>29,30</sup>. Sections were then washed with PBS-T three times and incubated in secondary antibodies diluted in blocking solution (donkey anti-rabbit, donkey anti-goat, Alexa Fluor 488 or 594, 1:500; Thermo Fisher, A11055, R37118, R37119) with DAPI (1:20000; Thermo Fisher, D1306) or NeuroTrace 435/455 Blue Fluorescent Nissl Stain (1:200; Thermo Fisher, N21479) for 2–3 hours at room temperature. Sections were then washed with PBS for three times, mounted on Superfrost slides (Fisher scientific, 12–550-15) and coverslipped for imaging on a confocal microscope (Zeiss LSM 510 or 700 microscope) and/or a virtual slide scanner (Olympus, VS120).

### Fluorescent *In situ* hybridization

Extracted brains were frozen on dry ice and 12- $\mu$ m coronal brain sections were collected using a cryostat (Leica Biosystems). For all genes except *Pde11a*, we performed RNAscope labeling following the manufacturer protocol (ACD; Advanced Cell Diagnostics)<sup>36</sup>. For Alexa555-CTB labeled tissues, incubation time for protease solution IV was shortened from 30 min to 30 s to preserve Alexa555-CTB expression. For *Pde11a*, RNA probes were generated from the pSPT19 Vector (Sigma) using primers reported on [www.brain-map.org](http://www.brain-map.org). Specifically, pSPT19 plasmid was cut with EcoRI and the antisense strand was transcribed using a T7 RNA polymerase with digoxigenin-labeled UTP (DIG RNA Labeling Kit; Sigma-Aldrich, 11175025910). The probe was then hybridized with the sample at 56 °C for 16 h, detected with horseradish peroxidase-conjugated anti-DIG antibody (1:500; Sigma-Aldrich, 11207733910)<sup>54</sup>, amplified with biotin-conjugated tyramide (PerkinElmer, EL748001KT) and visualized with Alexa 488-conjugated streptavidin (Thermo Fisher, S32354)<sup>30</sup>.

### Cell counting and axon terminal quantification

To analyze labeled cells, 20  $\times$  confocal or epifluorescence images were acquired and cells were counted manually using ImageJ. Cells that were not entirely contained within a given region of interest (ROI) were excluded from analyses. For counting DAPI, Nissl, CTB<sup>+</sup>, Fos<sup>+</sup> and Esr1<sup>+</sup> cells, 20  $\times$  fluorescent confocal images were acquired. For counting GCaMP6<sup>+</sup>, EYFP<sup>+</sup> and mCherry<sup>+</sup> in dual retrograde labeling, pharmacogenetics and fiber photometry experiments, 20  $\times$  fluorescent images were acquired with a virtual slide scanner (Olympus, VS120). For Figure 1k, PA in each brain section was divided to four quadrants along the long and short axes. Then, labeled cells in each quadrant were counted and the sum from all sections (6–7 sections, 50  $\mu$ m/section, ranging from Bregma –2.15 mm to –2.90 mm) was calculated and averaged across animals. For dual retrograde labeling, all mCherry<sup>+</sup> and EYFP<sup>+</sup> neurons in the amygdala were counted. For monosynaptic rabies tracing, all GFP<sup>+</sup> cells throughout the brain were counted except those in the primary infection site. Figure 7c and 7h includes areas that contribute to >1% of total inputs to PA<sup>Esr1+MPN</sup> or PA<sup>Esr1+VMHvl</sup> cells. To quantify the density of the projections of PA<sup>Esr1+MPN</sup> and PA<sup>Esr1+VMHvl</sup> cells, we selected a boxed area (200  $\times$  200  $\mu$ m for AVPV, VMHvl, PMv and LSv, 300  $\times$  400  $\mu$ m for MPN, 250  $\times$  250  $\mu$ m for MeApd, 250  $\times$  400  $\mu$ m for BNSTpr, 300  $\times$  200  $\mu$ m for vSub) in each region containing fibers and calculated the average pixel intensity as  $F_{raw}$  using ImageJ

and Photoshop. On the same image, a boxed area of the same size but in a brain region containing no fiber terminals was selected for calculating the background intensity ( $F_{\text{background}}$ ).  $F_{\text{signal}}$  was then calculated as  $F_{\text{raw}}$  minus  $F_{\text{background}}$ . For each animal,  $F_{\text{signal}}$  was normalized by the maximum  $F_{\text{signal}}$  across all the analyzed regions. The normalized  $F_{\text{signal}}$  was then used for calculating the average terminal field intensity across animals.

### ***In vitro* electrophysiological recordings**

*Esr1-2A-Cre* male adult mice were injected with 140 nL AAV2-Ef1 $\alpha$ -DIO-ChR2-EYFP into the PA and 100 nL AAV2-hSyn-DIO-mCherry into MPN and VMHv1. Three weeks after virus injection, acute coronal brain slices of MPN and VMHv1 (275  $\mu\text{m}$  in thickness) were obtained using standard methods as described previously<sup>29</sup>. Briefly, isoflurane-anesthetized mice were perfused with ice-cold artificial cerebrospinal fluid (ACSF) containing (in mM) 125 NaCl, 2.5 KCl, 1.25 NaH<sub>2</sub>PO<sub>4</sub>, 25 NaHCO<sub>3</sub>, 1 MgCl<sub>2</sub>, 2 CaCl<sub>2</sub> and 11 glucose. Slices were collected in ice-cold choline-based cutting solution (in mM: 110 choline chloride, 25.0 NaHCO<sub>3</sub>, 2.5 KCl, 7 MgCl<sub>2</sub>, 0.5 CaCl<sub>2</sub>, 1.25 NaH<sub>2</sub>PO<sub>4</sub>, 25.0 glucose, 11.6 ascorbic acid, and 3.1 pyruvic acid) using a Leica VT1200s vibratome, incubated for 10–20 min in ACSF at 34°C and then at room temperature until use. Individual slices were transferred to a recording chamber mounted on an upright microscope (Slicescope Pro 6000, Scientifica) and continuously perfused with ACSF warmed to 32–34°C (TC-344C; Warner Instruments). All solutions were constantly bubbled with 95% O<sub>2</sub>/5% CO<sub>2</sub>. mCherry-labeled *Esr1*<sup>+</sup> neurons within either MPN or VMHv1 were identified with an Olympus 40 $\times$  water-immersion objective using infrared differential interference contrast optics and epifluorescence. Standard whole-cell voltage-clamp recordings were performed using glass electrodes (2–4 M $\Omega$ ) containing (in mM) 135 CsMeSO<sub>3</sub>, 10 HEPES, 1 EGTA, 3.3 QX-314 (Cl<sup>-</sup> salt), 4 Mg-ATP, 0.3 Na-GTP, and 8 Na<sub>2</sub>-Phosphocreatine (pH 7.3 adjusted with CsOH). Series resistance did not exceed 20 M $\Omega$ . Membrane currents were amplified and low-pass filtered at 3 kHz using a Multiclamp 700B amplifier (Molecular Devices), digitized at 10 kHz and acquired using National Instruments acquisition boards (PCIe-6351 and PCI-6713) and a custom version of ScanImage (<https://github.com/bernardosabatini/SabalabAcq>) written in MATLAB (Mathworks) and analyzed offline using Igor Pro (Wavemetrics). To activate ChR2-expressing axons, brief pulses of full field illumination (1 ms duration; 10 mW $\cdot\text{mm}^{-2}$  under the objective) were delivered onto the recorded cell with a blue LED light (pE-300white; CoolLED) at 30 s intervals. Optogenetically-evoked EPSCs and IPSCs (oEPSPs and oIPSCs) were recorded by holding the membrane potential of recorded neurons at  $-70$  and  $0$  mV (corrected for a  $\sim 8$  mV liquid junction potential), respectively. 10  $\mu\text{M}$  6-cyano-7-nitroquinoxaline-2,3-dione (CNQX; Tocris, 190) was bath applied to confirm that oEPSC is mediated by AMPA receptor and the oIPSC is polysynaptic and dependent on the oEPSC.

### **Behavioral analysis**

Animal behaviors in all experiments were video recorded from both the side and top of the cage using two synchronized cameras (Basler, acA640–100 gm) and a commercial video acquisition software (StreamPix 5, Norpix) in a semi-dark room with infrared illumination at a frame rate of 25 frames/s. Behavioral annotation and tracking were performed on a frame-by-frame basis using custom software written in MATLAB (<https://pdollar.github.io/>

toolbox)<sup>6</sup>. For male sexual behaviors, “Attempt mount” was defined as when the male extends his forelimbs to grasp and mount the female’s flanks. “Shallowly thrust” was defined as when the male poses his forelegs over the female’s back and with his hindlimbs on the ground accompanying shallow pelvic thrusts. The “Shallowly thrust” onset was defined as the moment when the male begins to rapidly thrust against the female’s rear. “Deeply thrust” was defined as a deep rhythmic thrust following “Shallow-thrust”. The onset of “Deeply thrust” was defined as the time when the male performs the first deep-thrust, presumably inserting its penis into the female’s vaginal part. “Ejaculate” was detected when the male stops deep thrusting for seconds while continuously clutching onto the female and then slumps to the side of the female. The putative ejaculation event was confirmed by the presence of vaginal copulatory plug after the test. For aggression, attack was defined by a suite of actions initiated by the resident toward the male intruder, which included lunges, bites, tumbling, and fast locomotion episodes between such behaviors. Sniffing was defined by nose contact to the foreign body. Mouse behavior was manually annotated frame-by-frame by an experimenter not blind to the group assignment of the animals. Attack events in a randomly selected set of videos were annotated using Deeplabcut<sup>55</sup> and Simba<sup>56</sup> and good agreement between human and machine annotations was observed. During annotation, the neural responses were not available to the experimenter.

### Fiber photometry

The test animals were screened for both aggressive behaviors and sexual behaviors before the surgery and randomly assigned to experimental and control groups. Fiber photometry was performed as described previously<sup>10,29,30</sup>. Briefly, a 390-Hz sinusoidal blue LED light (30  $\mu$ W) (LED light: M470F1; LED driver: LEDD1B; both from Thorlabs) were bandpass filtered (passing band:  $472 \pm 15$  nm, FF02–472/30–25, Semrock) and delivered to the brain to excite GCaMP6. The emission lights traveled back through the same optic fiber, bandpass filtered (passing bands:  $535 \pm 25$  nm, FF01–535/505, Semrock), passed through an adjustable zooming lens (Thorlab, SM1NR01 and Edmund optics, #62–561), detected by a Femtowatt Silicon Photoreceiver (Newport, 2151) and recorded using a real-time processor (RZ5, TDT). The envelope of the 390-Hz signals reflected the intensity of the GCaMP6 and was extracted in real time using a custom TDT OpenEx program. The signal was low pass filtered with a cut-off frequency of 5 Hz. During recording, a sexually receptive female C57BL/6N mouse (‘intruder’) was placed in the homecage of the experimental male mouse (‘resident’) until the resident reached ejaculation. After the session with a female intruder, a group housed non-aggressive male BALB/c or C57BL/6N mouse was placed in the homecage for 10 minutes and then an object was introduced into the home cage of the recorded male for 5 minutes. Each stimulus was presented with three minutes in between. To analyze the recording data, the MATLAB function “msbackadj” with a moving window of 25% of the total recording duration was first applied to obtain the instantaneous baseline signal. The instantaneous  $F/F$  was calculated as  $(F_{\text{raw}} - F_{\text{baseline}})/F_{\text{baseline}}$ . The peri-event histogram (PETH) of a given behavior was constructed by aligning the  $F/F$  signal to the onset of the behavior. The  $F/F$  values during ‘Attempted-mount’ and ‘Shallow-thrust’ was calculated based on trials that were not followed by ‘Deep-thrust’. The peak  $F/F$  for each behavior episode were calculated as the maximum  $F/F$  of the PETHs during each behavioral episodes minus the average  $F/F$  in the duration-matched period prior to the

behavior onset. The resulted values of all behavior episodes of the same behavior were then averaged for each animal and plotted in Figure 4z. The location of the animals were tracked using a custom software (<https://github.com/pdollar/toolbox>)<sup>6,57</sup>. The velocity of the animal was calculated as the displacement of the animal location between two adjacent frames. The change points in velocity were determined using Matlab function “findchangepts”. Only change points after a period (>2s) of immobility (velocity < 2pixels/frame) were included for analysis. We separated the change points based on whether a mounting attempt occurred within 3s or not and calculate the average Ca<sup>2+</sup> signal change between -1-0s and 0-1s of the change points followed by or not followed by sexual behaviors.

### Pharmacogenetic neural silencing

The test animals were screened for both aggressive behaviors and sexual behaviors before the surgery and randomly assigned to experimental and control groups. For PA<sup>Esr1+</sup> inactivation experiments, we screened the sexual performance of the animals before and two weeks after surgery to ensure the high sexual performance. During screening, a receptive C57BL/6N female (predetermined using a highly sexually experienced male) was introduced into the home cage of the test mouse and only animals achieved intromission during the 10 minutes test periods were included in the final test. Three weeks after the injection, mice were intraperitoneally injected with saline and CNO (5 mg/kg, Sigma, C0832) on interleaved day. 30 min after saline or CNO injection, a sexually receptive female C57BL/6N mouse was placed in the homecage of the test mouse and test mouse was allowed to freely interact with the female for 10 minutes or until the male showed 15 times of attempted mounting or 10 times of intromission, whichever is shorter. For PA<sup>Esr1+MPN</sup> and PA<sup>Esr1+VMHvl</sup> inactivation experiments, males are screened for both aggressive behaviors and sexual behaviors both before and two weeks after the surgery. During aggression screening, a group-housed BALB/c male mouse was introduced into the home cage of the test mouse and only animals showed minimum 5 attacks during the 10 minutes testing period were included in the final test. Three weeks after the surgery, the sexual and aggressive behaviors were tested after CNO and saline injection. During each test, the test mouse encountered a receptive female first for maximally 10 minutes (see above) and a non-aggressive BALB/c male mouse for 10 minutes after the female was removed for three minutes.

### Pharmacogenetic neural activation

For PA<sup>Esr1+MPN</sup> and PA<sup>Esr1+VMHvl</sup> activation experiments, test animals were naïve (no prior sexual experience or tested for aggression) and group housed before the virus injection and singly housed after surgery. Animals were assigned to test and control groups randomly. Three weeks after the surgery, test males were intraperitoneally injected with saline and CNO (0.1 or 0.5 mg/kg, Sigma, C0832) on separate days. 30 min after saline or CNO injection, a non-receptive female and then a non-aggressive BALB/c male mouse was introduced to the home cage of the test animal, each for 10 minutes with 2 minutes in between. Note that no test animal achieved deep thrust in this experiment as the female is non-receptive.

## Intersectional optogenetic behavioral experiments

Test animals were naïve (no prior sexual experience or tested for aggression) and group housed before the virus injection and singly housed after surgery. Animals were assigned to test and control groups randomly. After three weeks of viral incubation, on the test days, two 200- $\mu\text{m}$  multimode optical fibers (Thorlabs, FT200EMT) were connected with the bilateral implanted ceramic ferrules (Thorlabs, CFLC230–10) using a match sleeve (Thorlabs, ADAL1). Randomly selected group-housed adult BALB/c male, castrated BALB/c male, C57BL/6N female mice were introduced into the home cage of the subject. Blue light (473 nm, Shanghai Dream Laser) was delivered through the fiber bilaterally in 20 ms pulses at 20 Hz with the intensity ranging from 0.5 to 7.5 mW for 60 s using OpenEx (TDT). The light intensity was measured at the fiber end during pulsing using an optical power meter (Thorlabs, PM100D). A sham stimulation period (0 mW) for 60–180 s was interleaved with the real light stimulation period as an internal control. All behavioral tests were repeated at least once to ensure the reproducibility of any light-induced behavioral changes in the same session.

## Subpopulation specific input and output mapping

To investigate downstream targets of  $\text{PA}^{\text{Esr1+MPN}}$  and  $\text{PA}^{\text{Esr1+VMHvl}}$  cells, the brain was harvested for histological analysis after two weeks of viral incubation. Every third section (50- $\mu\text{m}$  thickness) was collected and immunohistochemistry was performed to amplify eGFP signals in neuronal fibers in downstream areas.

To map the inputs to  $\text{PA}^{\text{Esr1+MPN}}$  and  $\text{PA}^{\text{Esr1+VMHvl}}$  cells, we induced cell-type-specific TRIO (tracing the relationship between input and output) method<sup>41</sup>. One week after rabies injection, the brain was harvested for histological analysis. Every third section (50- $\mu\text{m}$  thickness) was quantitated and all GFP-positive input cells were counted excluding the site of EnvA-G-Deleted Rabies-eGFP injection.

## LCM RNA-Seq

Red and Green retrobeads (Lumaflo Item, R170 and G170) were injected into the ipsilateral MPN and VMHvl in C57BL/6N mice, respectively. One week later, mice were deeply anesthetized with isoflurane and brains were harvested and flash frozen in chilled 2-methylbutane (approximately  $-80\text{ }^{\circ}\text{C}$ ) within 5 min and stored at  $-80\text{ }^{\circ}\text{C}$  until sectioning. 20- $\mu\text{m}$  coronal sections were obtained using a cryostat and mounted on PEM membrane slides (Leica microsystems, 11505189). The slides were pretreated with 100% ethanol for 1 min and air dried.  $\text{PA}^{\text{MPN}}$  and  $\text{PA}^{\text{VMHvl}}$  subpopulations were laser-dissected based on the retrograde labeling using a LMD6000 fluorescence microscope system (Leica microsystems). The RNA samples and cDNA libraries were prepared with a PicoPure RNA isolation kit (ThermoFisher, KIT0204) and Clontech SMARTer Stranded Total RNA-Seq Kit (Cat# 635006) as previously described<sup>30</sup>. The cDNA libraries were sequenced with Illumina HiSeq 4000 using high output mode to achieve greater depth of coverage. Sequencing reads were aligned to the mouse genomes (build mm10/GRCm38) using the splice-aware STAR aligner<sup>58</sup> and then the counts for each gene were generated using featureCounts<sup>59,60</sup>. Differential gene expression analysis between PA and BMAp or  $\text{PA}^{\text{MPN}}$  and  $\text{PA}^{\text{VMHvl}}$  populations was performed using the limma R package<sup>61</sup> with normalized gene reads

through an open-source software iDEP (<http://ge-lab.org/idep/>)<sup>62</sup>. We selected whole PA region enriched genes with a threshold of false discovery rate (FDR) < 0.05 and fold-change > 1.5 between PA and BMAp populations, and subpopulation-specific genes in the PA with FDR < 0.07 and fold-change > 1.5 between PA<sup>MPN</sup> and PA<sup>VMHvl</sup> populations.

## Statistics

All statistical analyses for histological, *in vivo* and *in vitro* recording and behavioral experiments were performed using MATLAB2018a (Mathworks) or Prism7 software (GraphPad). Except for repeated measure two-way ANOVA, all data sets were tested for normality with Kolmogorov-Smirnov test. For one-way ANOVA, Brown-Forsythe test was used to test equality of variances. If the data set passed the normality test, parametric tests (unpaired *t*-test, paired *t*-test, repeated measure and ordinary one-way ANOVA with Geisser-Greenhouse correction and Turkey's multiple comparison post-hoc test, ordinary two-way ANOVA with Bonferroni's multiple comparison post-hoc test) were used, otherwise, non-parametric tests (Mann Whitney test, Wilcoxon matched-pairs signed rank test, Friedman test with Dunn's multiple comparison post-hoc test) were used. Following repeated measure two-way ANOVA, post-hoc Bonferroni's multiple comparison test was performed. Differential gene expression between brain regions was analyzed by two-tailed *t*-test with Benjamini-Hochberg false discovery rate correction. All significant statistical results were indicated on the figures with the following conventions: \**p* < 0.05, \*\**p* < 0.01, \*\*\**p* < 0.001, \*\*\*\**p* < 0.0001. All error bars represent ± s.e.m. No statistical methods were used to pre-determine sample sizes but our sample sizes are similar to those reported in previous publications<sup>6,7,9,14,29,30</sup>. Additional details of statistics can be found in Supplementary Table 1.

## Life Sciences Reporting Summary

Further information on research design is available in the Nature Research Reporting Summary linked to this article.

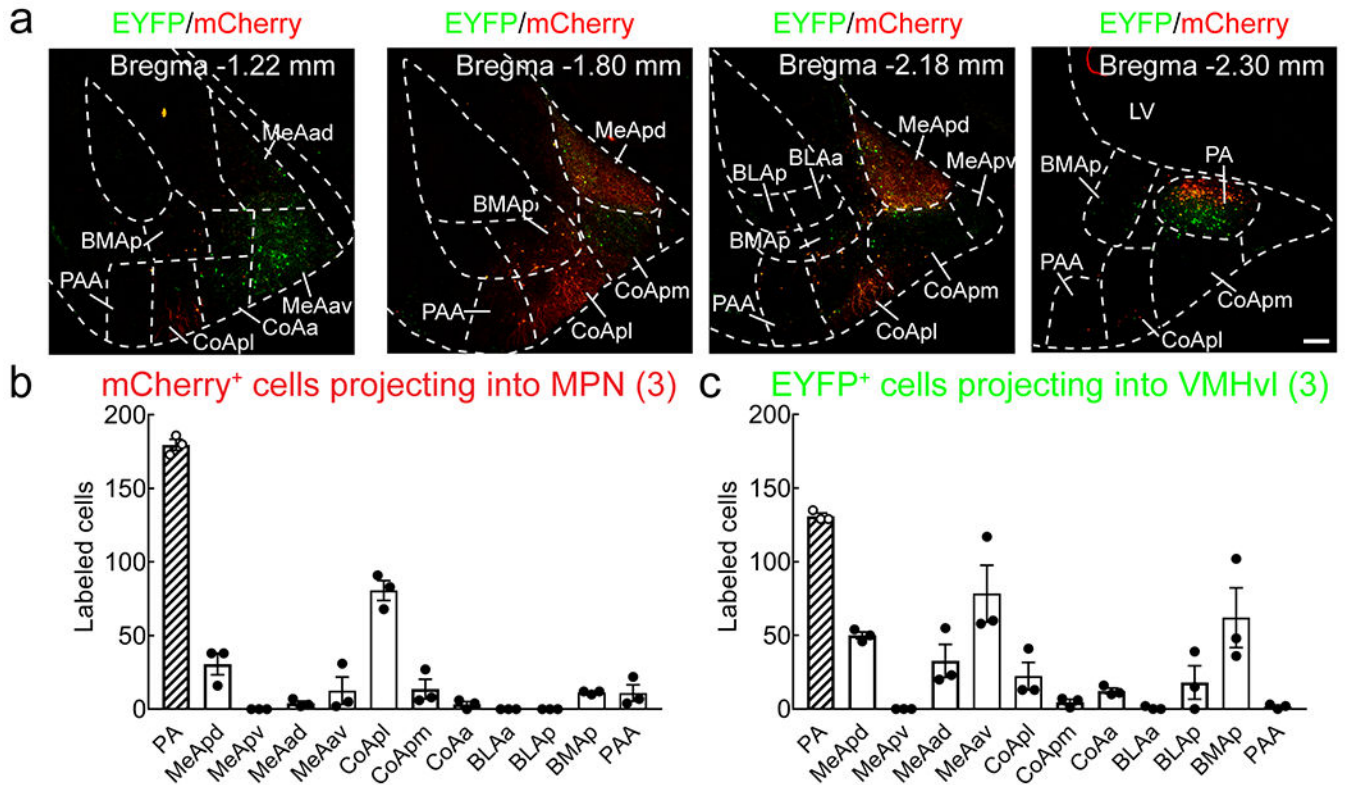
## Data availability

We have uploaded the RNAseq data from this manuscript to the Gene Expression Omnibus (GEO) under accession number GSE 151798. All other data that support the findings of this study are available from the corresponding authors upon request.

## Code availability

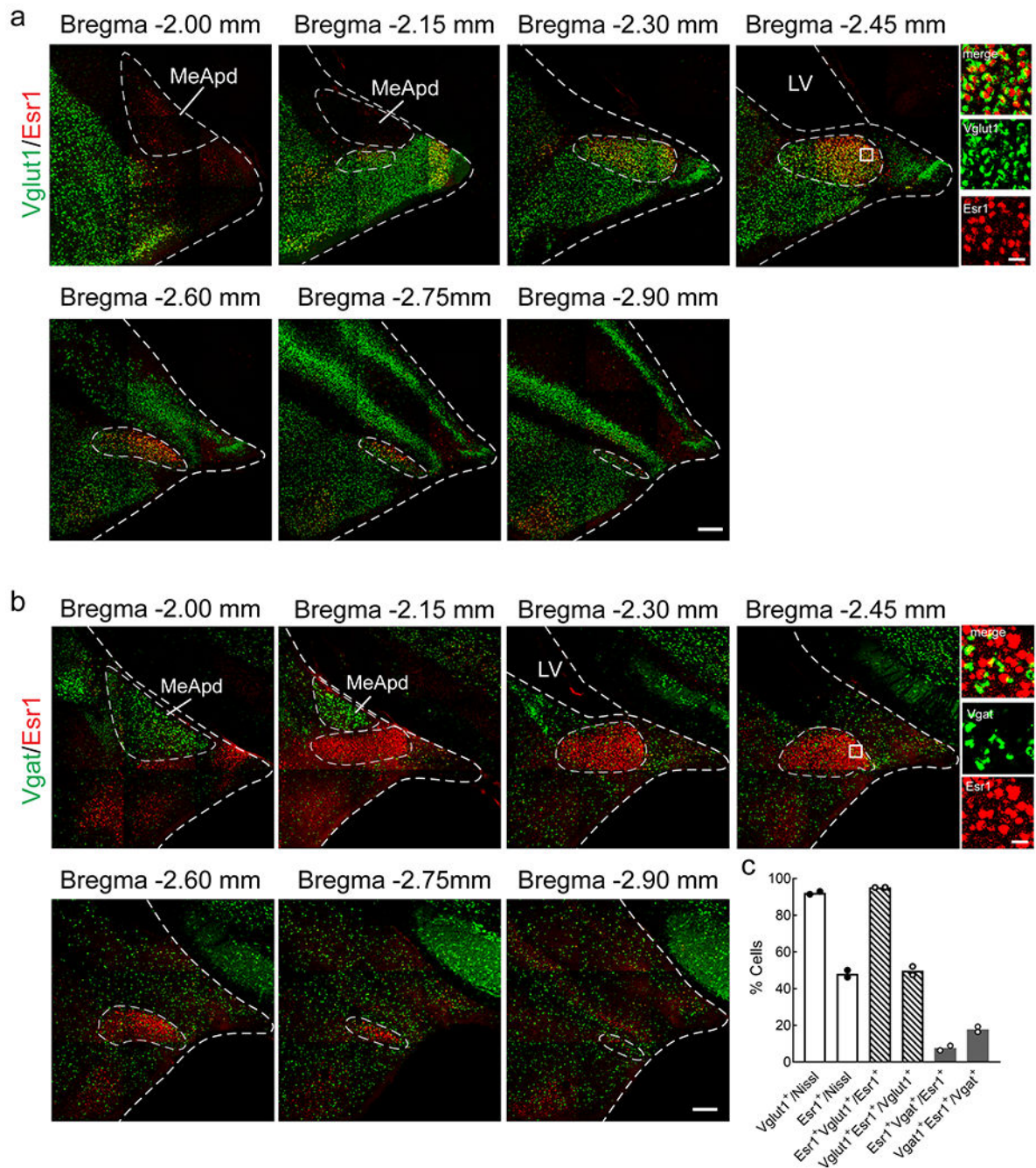
MATLAB code ScanImage is available at <https://github.com/bernardosabatini/SabalabAcq>. MATLAB codes for behavioral annotation and tracking are available from <https://github.com/pdollar/toolbox>. Custom TDT OpenEx programs and MATLAB codes for fiber photometry data analysis will be provided upon request to the corresponding authors.

## Extended Data



**Extended Data Fig. 1. PA<sup>Esr1+</sup> cells provide the largest inputs to the medial hypothalamus among all the *Esr1*<sup>+</sup> cells in the amygdala, related to Figure 1.**

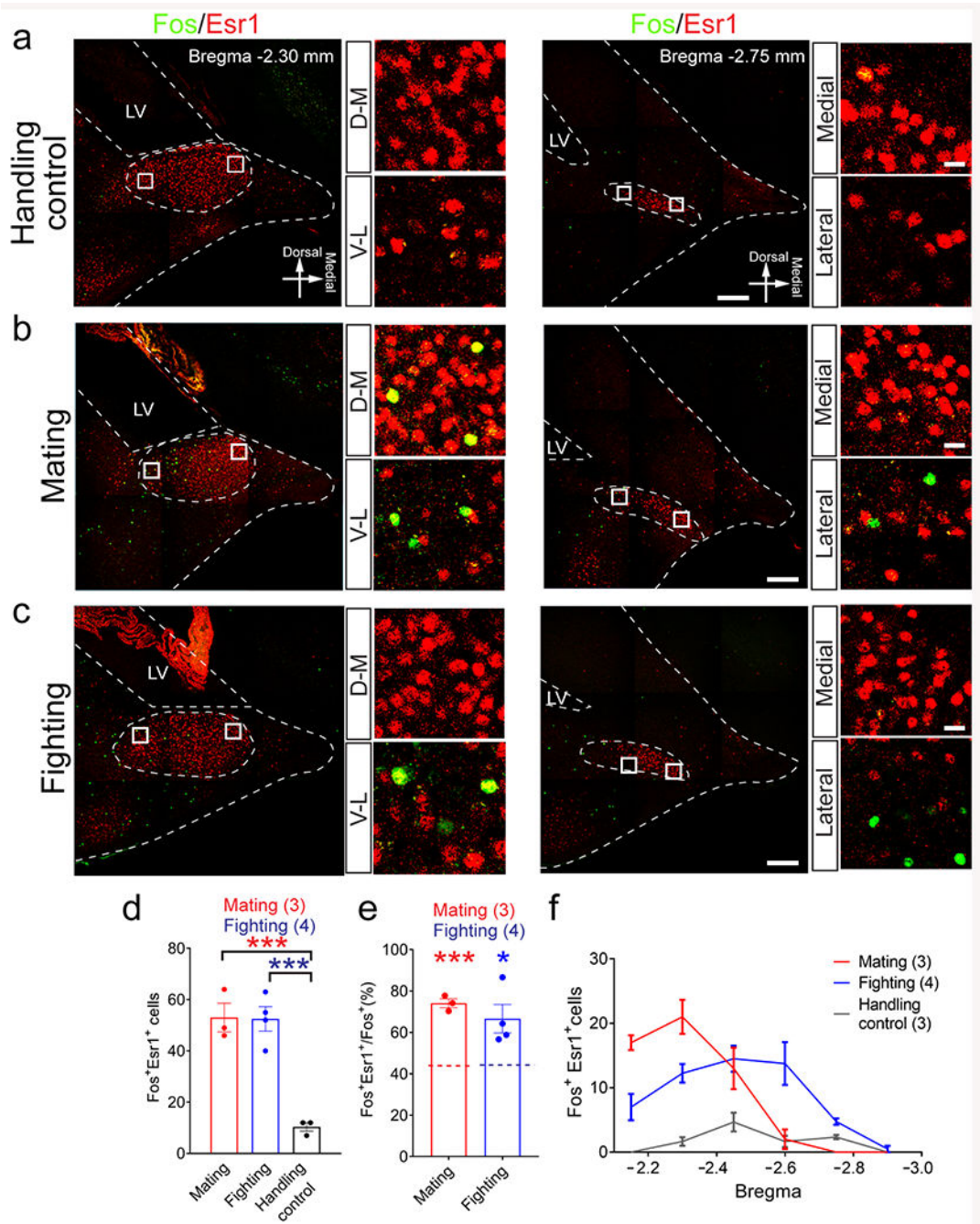
(a) The retrogradely labeled *Esr1*<sup>+</sup> cells in the amygdala after HSV injection into VMHvl (green) and MPN (red). Scale bar: 200  $\mu$ m. Images are representative of  $n = 3$  mice. (b and c) The distributions of mCherry<sup>+</sup> (MPN projecting, b) and EYFP<sup>+</sup> cells (VMHvl projecting, c) after injecting HSV-hEfl $\alpha$ -LS1L-mCherry into the MPN and HSV-hEfl $\alpha$ -LS1L-EYFP into the VMHvl of *Esr1-2A-Cre* male mice. Data in b and c are presented as mean  $\pm$  s.e.m. PA: posterior amygdala; MeApd: medial amygdala posterior dorsal subdivision; MeApv: medial amygdala posterior ventral subdivision; MeAad: medial amygdala anterior dorsal subdivision; MeAav: medial amygdala anterior ventral subdivision; CoApl: cortical amygdala posterolateral part; CoApm: cortical amygdala posteromedial part; CoAa: cortical amygdala anterior part; BLAa: basolateral amygdala anterior part; BLAp: basolateral amygdala posterior part; BMAP: basomedial amygdala posterior part; PAA: **piriform-amygdalar area**.



**Extended Data Fig. 2. Characterization of the neurotransmitter type of PA<sup>Esr1+</sup> neurons, related to Figure 2.**

(a and b) Overlay between Vglut1 (a) or Vgat (b) (green) and Esr1 (red) in the PA from bregma level -2.00 to -2.90 mm. Vglut1 and Vgat are visualized using *Vgat-ires-Cre* × Ai6 and *Vglut1-ires-Cre* × Ai6 lines, respectively. Right showing the enlarged view of the boxed area. Scale bars: 200 μm (bottom) and 20 μm (upper right). (c) The percentage of Vglut1<sup>+</sup> and Esr1<sup>+</sup> cells in the total neuronal populations in PA, the percentage of PA<sup>Esr1+</sup> cells that are glutamatergic or GABAergic, and the percentage of glutamatergic cells expressing Esr1

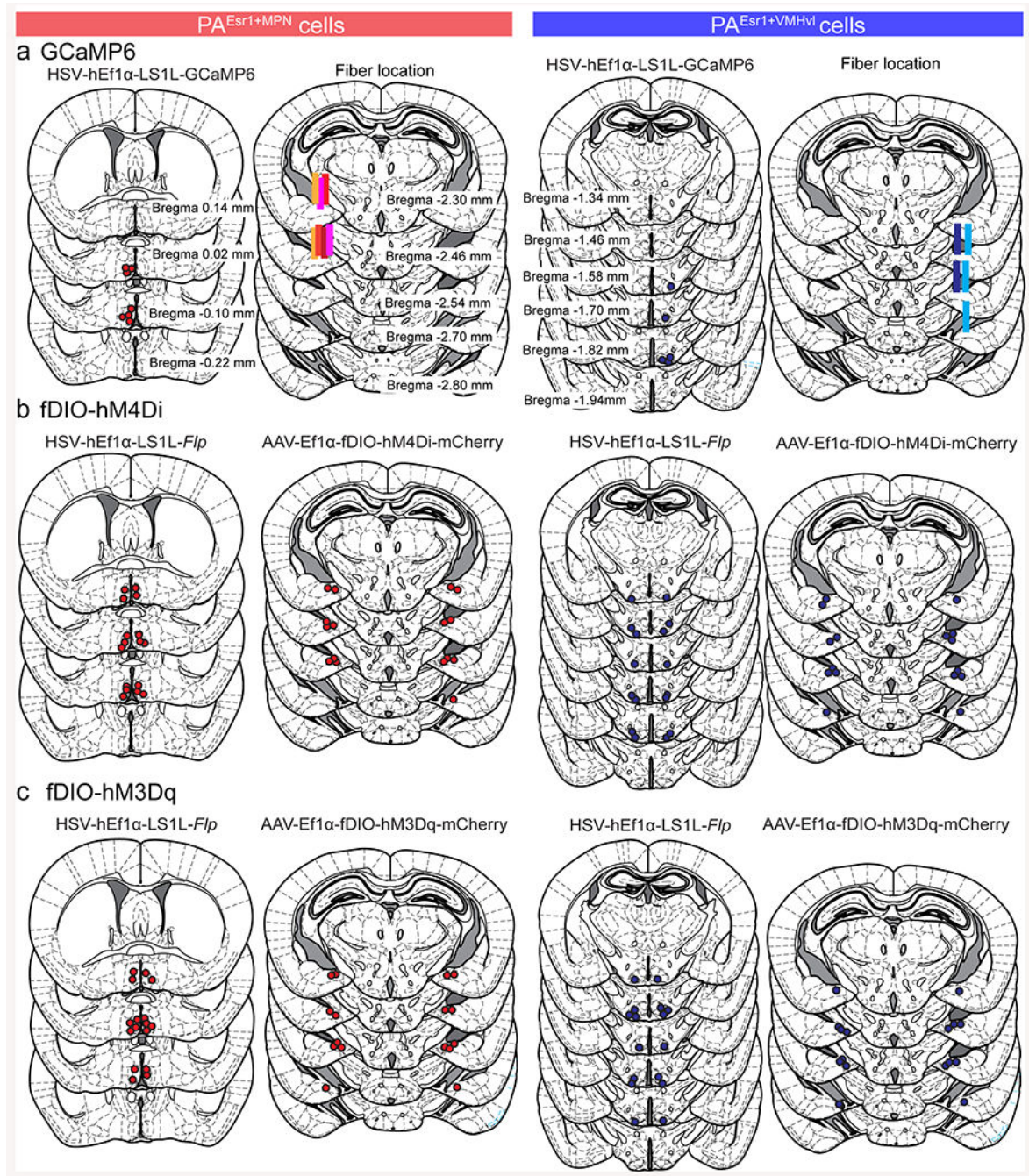
and the percentage of GABAergic cells expressing Esr1. n = 2 animals for each group. Data in c are presented as mean.



**Extended Data Fig. 3. Topographical Fos expression patterns in the PA after mating and fighting, related to Figure 4.**

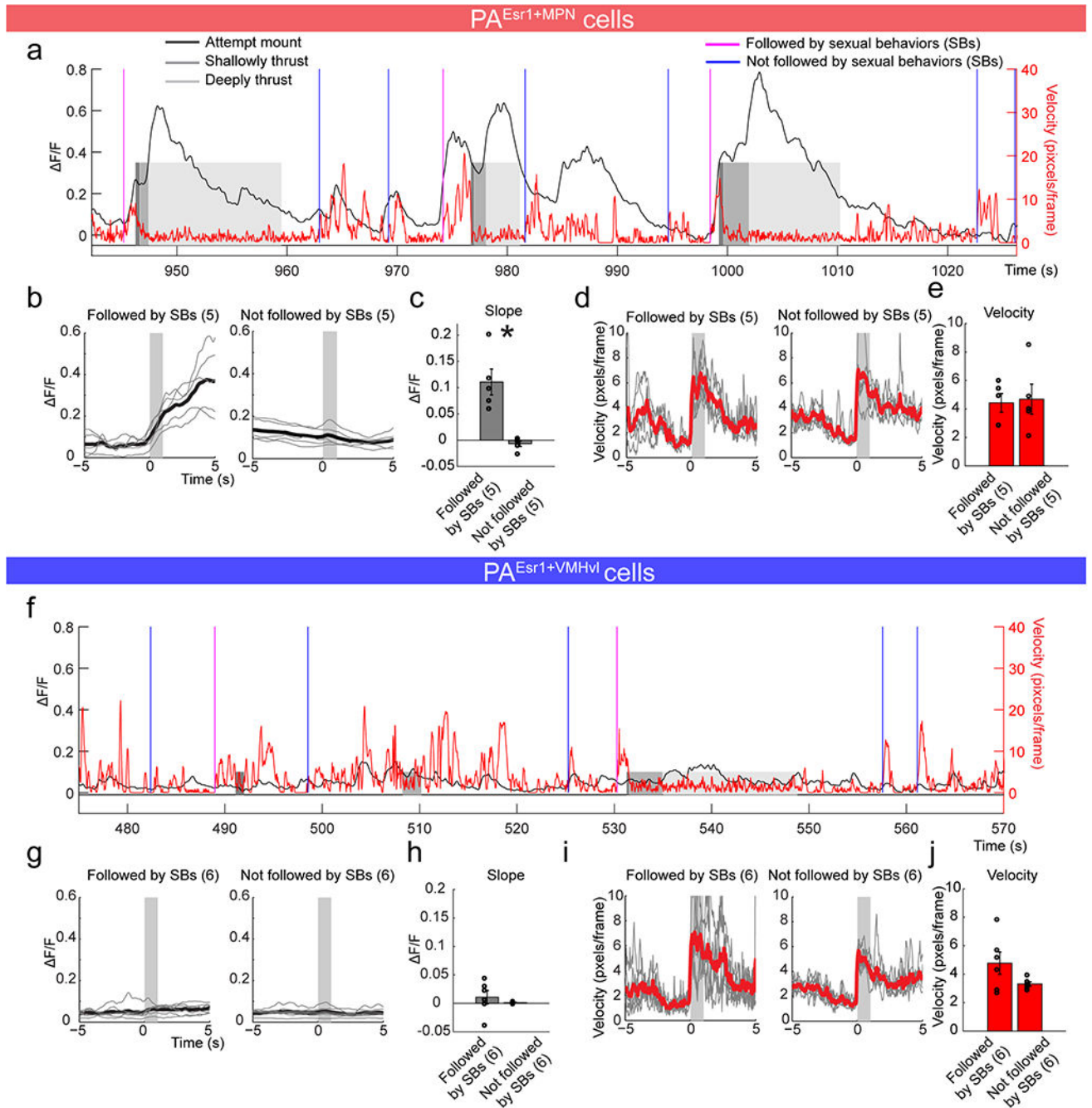
(a-c) Representative images showing the expression of c-Fos (green) and Esr1 (red) in the PA at bregma level -2.30 mm (left) and -2.75 mm (right) after handling (a) (n = 3 animals), mating (b) (n = 3 animals) or fighting (c) (n = 4 animals). Right showing the enlarged views of the boxed areas. Scale bars: 200 μm (left) and 20 μm (right). (d) The number of Fos<sup>+</sup>

neurons in the PA increased significantly after mating and fighting. One-way ANOVA with Tukey's multiple comparison test. (e) Majority of Fos<sup>+</sup> cells induced by mating or fighting express Esr1 in the PA. Red and blue dashed lines mark the percentage of Esr1<sup>+</sup> cells in the total PA population. Two-tailed unpaired t-test. (f) The number of Fos<sup>+</sup> neurons expressing Esr1 in the PA along the anterior-posterior axis after handling control (gray), mating (red) or fighting (blue). All data in d, e, and f are presented as mean ± s.e.m. \*p < 0.05, \*\*\*p < 0.001. For detailed statistics information, see Supplementary Table 1.



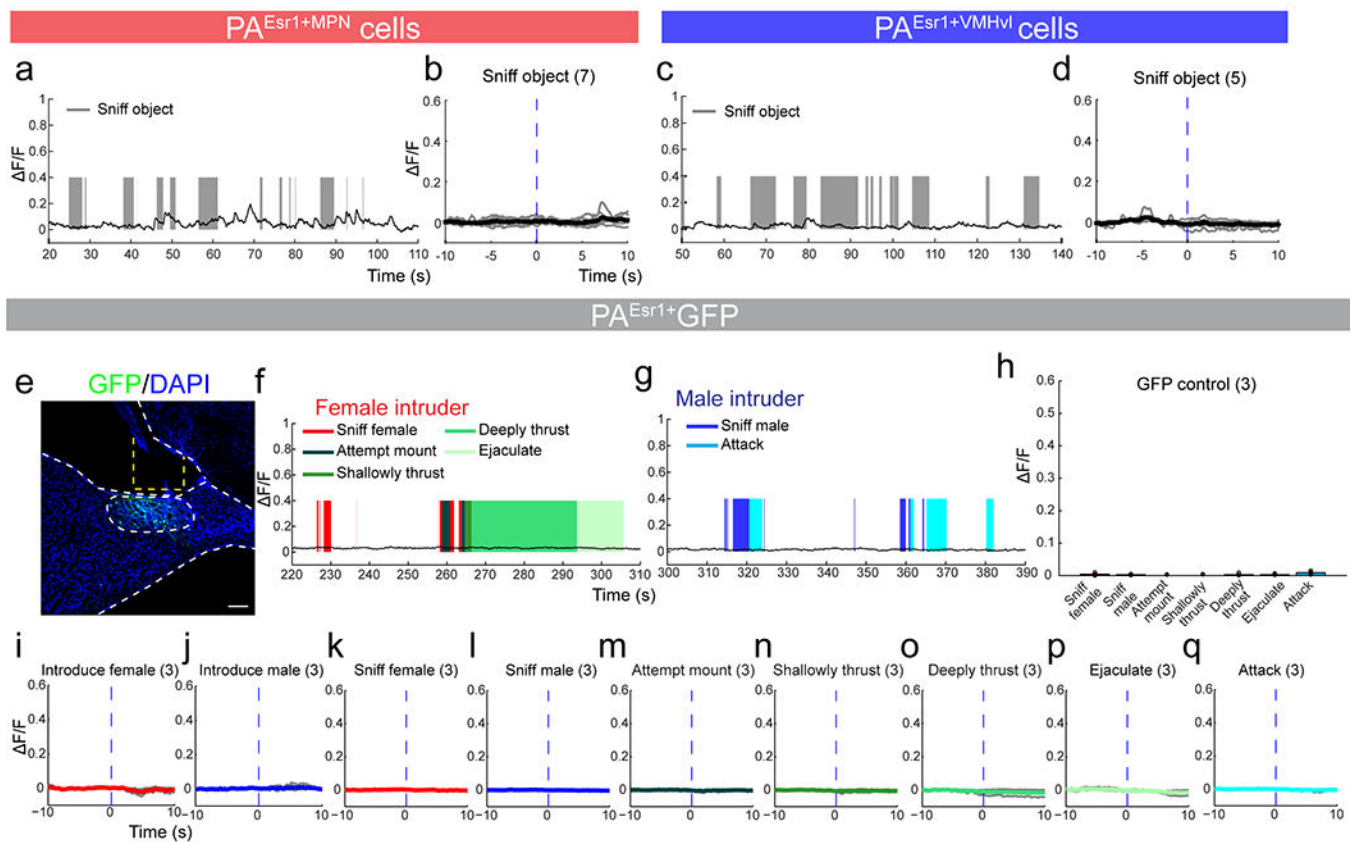
**Extended Data Fig. 4. Virus injection and expression sites and optic fiber placements for recording and functional manipulation experiments, related to Figures 4, 5 and 6.**

(a-c) Coronal brain sections at the bregma level of MPN, VMHvl and PA showing the virus injection or expression sites (dots) and optic fiber placements (lines) in fiber photometry and pharmacogenetics experiments. Each dot or line represents one animal. Injection and recording sites in each animal are unilateral in (a) and bilateral in (b and c). Brain atlas images are modified from<sup>51</sup>.



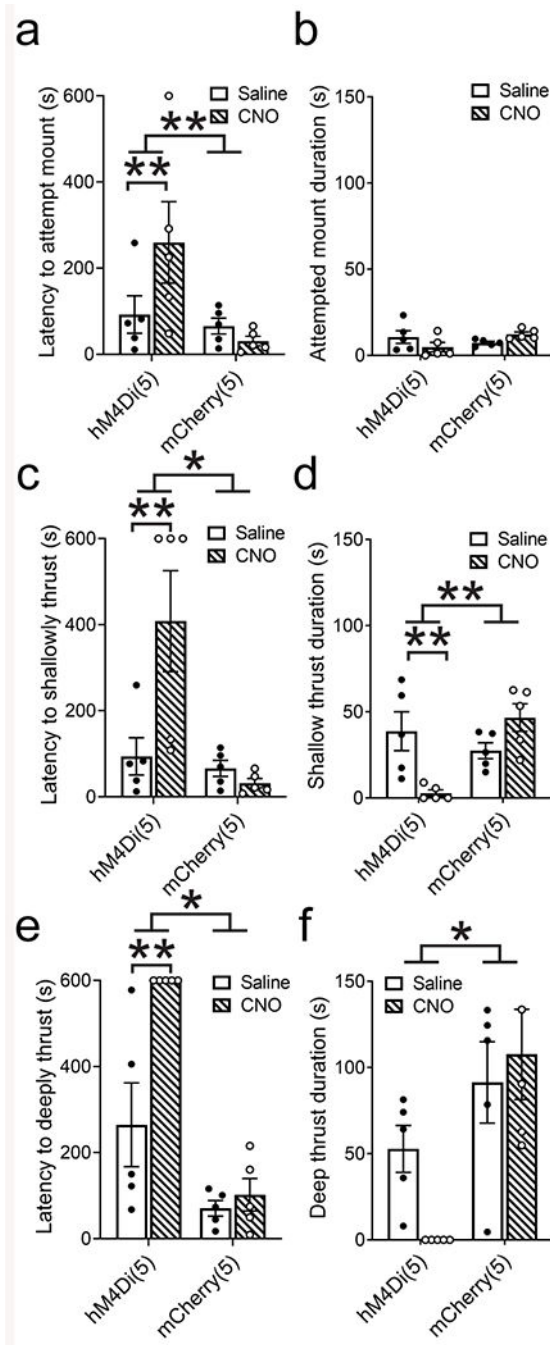
**Extended Data Fig. 5. PA<sup>Esr1+MPN</sup> cells but not PA<sup>Esr1+VMHvl</sup> cells increase activity during initiation of sexual behaviors, related to Figure 4.**

(a) Representative Ca<sup>2+</sup> trace (black) of PA<sup>Esr1+</sup> cells and the test animal's movement velocity (red) during interactions with a female mouse. Vertical lines mark the computer detected velocity changing points that are either followed by mounting attempts within 3 s (magenta) or not (blue). Gray shades mark the manually annotated attempted mount (dark gray), shallow-thrust (median gray) and deep-thrust (light gray). (b) Ca<sup>2+</sup> signal aligned to the onset of movement initiation, either followed by sexual behaviors (left) or not (right). (c) Bar graphs showing that the slope of the Ca<sup>2+</sup> signal is significantly positive between 0 and 1 s (shades in b) after movement initiation only if the animal later initiated mounting. The average latency from movement initiation to manually annotated mounting initiation is 1.3 s. (d) Velocity of the animal aligned to the automatically detected velocity changing points, either followed by sexual behaviors (left) or not (right). (e) Bar graphs showing the velocity change from -1-0 s to 0-1 s in (d) does not differ between trials followed by sexual behaviors and those not. n = 5 animals in b-e. (f-j) PA<sup>Esr1+VMHvl</sup> cells showed no increase in Ca<sup>2+</sup> activity during the movement initiation regardless whether it is followed by attempted mounting or not. Plots are organized in parallel to those shown in a-e. n = 6 animals in g-j. All data in c, e, h and j are presented as mean ± s.e.m. One sample two-tailed t-test in c and h. Two-tailed paired t-test in e and j. \**p* < 0.05. For detailed statistics information, see Supplementary Table 1.



**Extended Data Fig. 6. No change in PA<sup>Esr1+MPN</sup> and PA<sup>Esr1+VMHvl</sup> Ca<sup>2+</sup> signal during non-social interaction and no change in fluorescence signal during social behaviors in GFP control animals, related to Figure 4.**

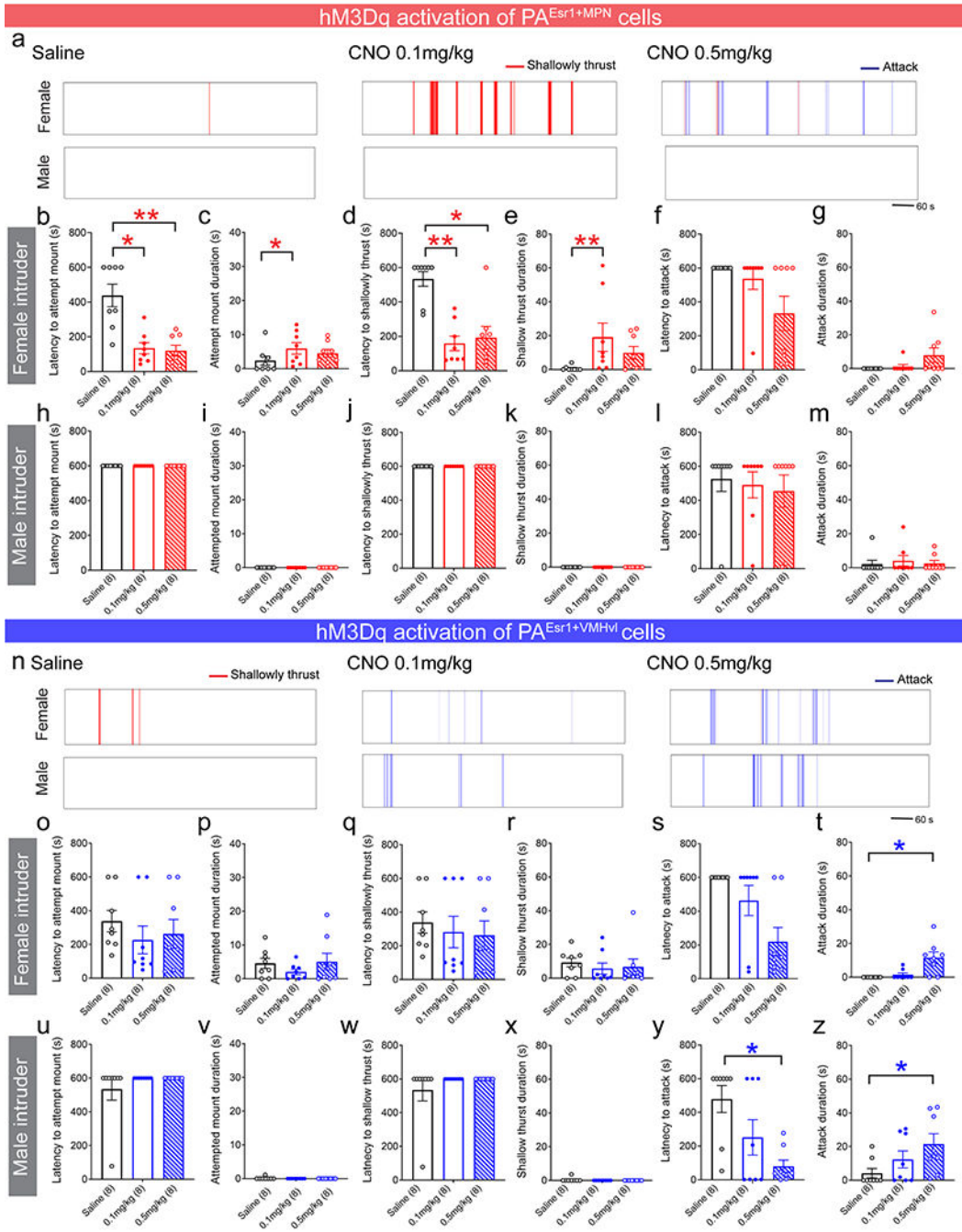
(a and c) Representative traces showing the GCaMP6 signal of PA<sup>Esr1+MPN</sup> (a) and PA<sup>Esr1+VMHvl</sup> (c) cells during object interaction. Gray shades mark sniffing object episodes. (b and d) PETHs of Ca<sup>2+</sup> signal ( $\Delta F/F$ ) of PA<sup>Esr1+MPN</sup> (b) and PA<sup>Esr1+VMHvl</sup> cells (d) aligned to sniffing object. n = 7 (PA<sup>Esr1+MPN</sup>) and 5 (PA<sup>Esr1+VMHvl</sup>) animals. (e) A representative image showing GFP (green) expression in the PA<sup>Esr1+</sup> cells. Blue: DAPI. Scale bar: 200  $\mu$ m. Yellow dashed lines indicate the optic fiber location. (f and g) Representative Ca<sup>2+</sup> traces during interaction with a female (f) and a male intruder (g) introduced into the home cage of the recording mouse. Colored shades mark the behavioral episodes. (h) The peak  $\Delta F/F$  during various social behaviors of all animals. n = 3 animals. All data in h are presented as mean  $\pm$  s.e.m. One-way ANOVA with post-hoc Tukey's test. p > 0.05. (i-q) PETHs of fluorescence signals aligned to intruder introduction (i and j), sniffing female (k), sniffing male (l), attempted mounting (m), shallow-thrust (n), deep-thrust (o), ejaculation (p), and attack (q). Gray and bold color lines indicate results from individual animals and the population average, respectively. Vertical dashed blue lines indicate time 0. For detailed statistics information, see Supplementary Table 1.



**Extended Data Fig. 7. hM4Di mediated  $PA^{Esr1+}$  cell inactivation impaired male mouse sexual behaviors. Related to Figure 5.**

(a, c, d) CNO injection prolonged the latencies to attempt mount (a), shallow thrust (c) and deep thrust (e) in  $PA^{Esr1+}$  hM4Di but not mCherry expressing animals. (b, d, f) The durations of shallow thrust (d) and deep thrust (f) significantly decreased after CNO injection in test but not control groups. Note that each test lasts 10 minutes. For animals that did not show the relevant behaviors within the testing period, the latency will be set at 600 s.  $n = 5$  animals in a-f. All data in a-f are presented as mean  $\pm$  s.e.m. Two-way ANOVA with

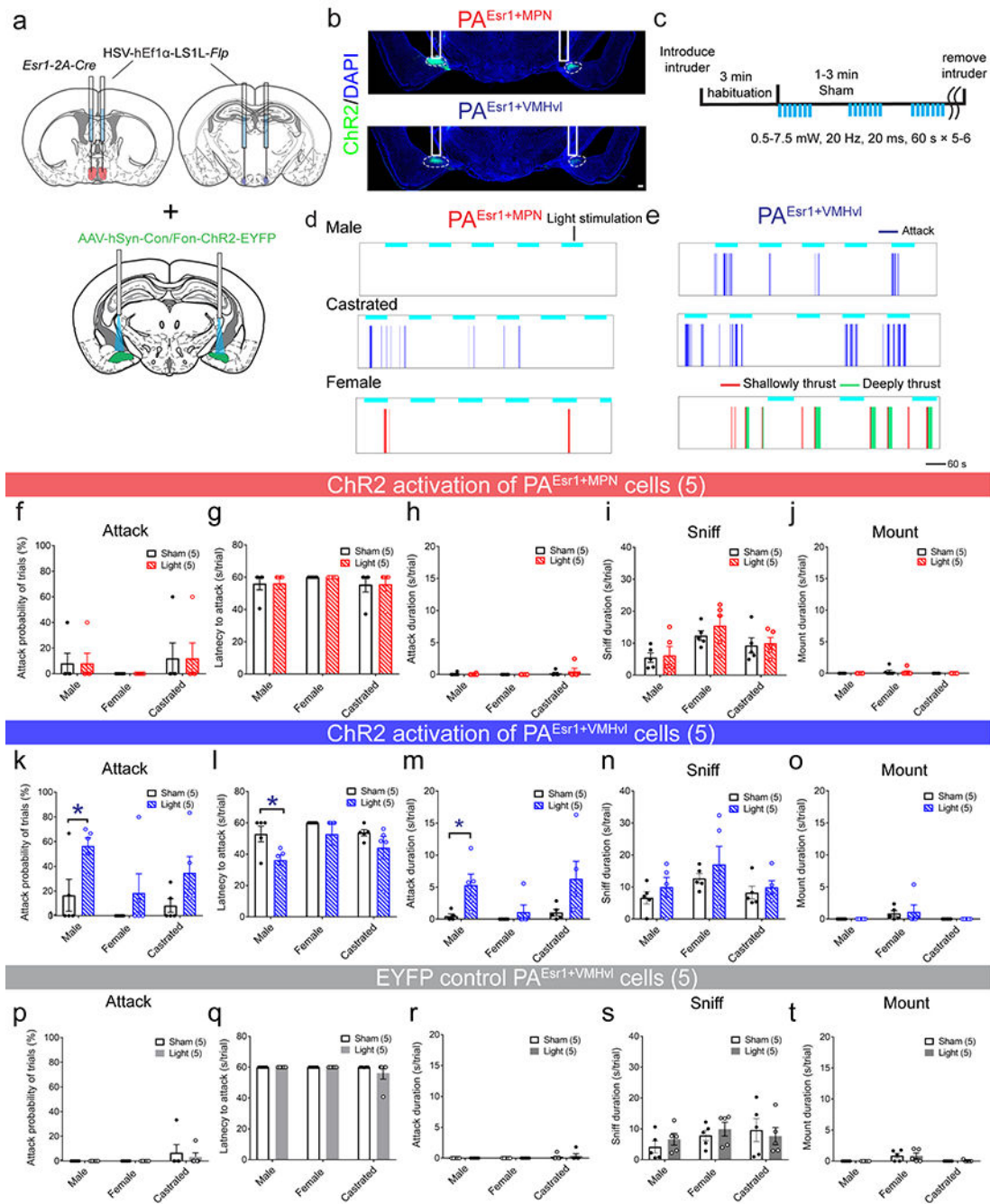
repeated measures followed by Bonferroni multiple comparison test. \* $p < 0.05$ ; \*\* $p < 0.01$ . For detailed statistics information, see Supplementary Table 1.



**Extended Data Fig. 8. hM3Dq mediated activation of PA<sup>Esr1+MPN</sup> and PA<sup>Esr1+VMHvl</sup> promote sexual and aggressive behaviors in naive male mice in a CNO dose dependent manner, related to Figure 6.**

(a) Representative raster plots showing the behaviors towards male and female intruders after saline, 0.1 mg/kg CNO and 0.5 mg/kg CNO i.p. injection in PA<sup>Esr1+MPN</sup> hM3Dq expressing animals. Scale bar: 60 s. (b-g) Both 0.1 mg/kg and 0.5 mg/kg CNO shortened the

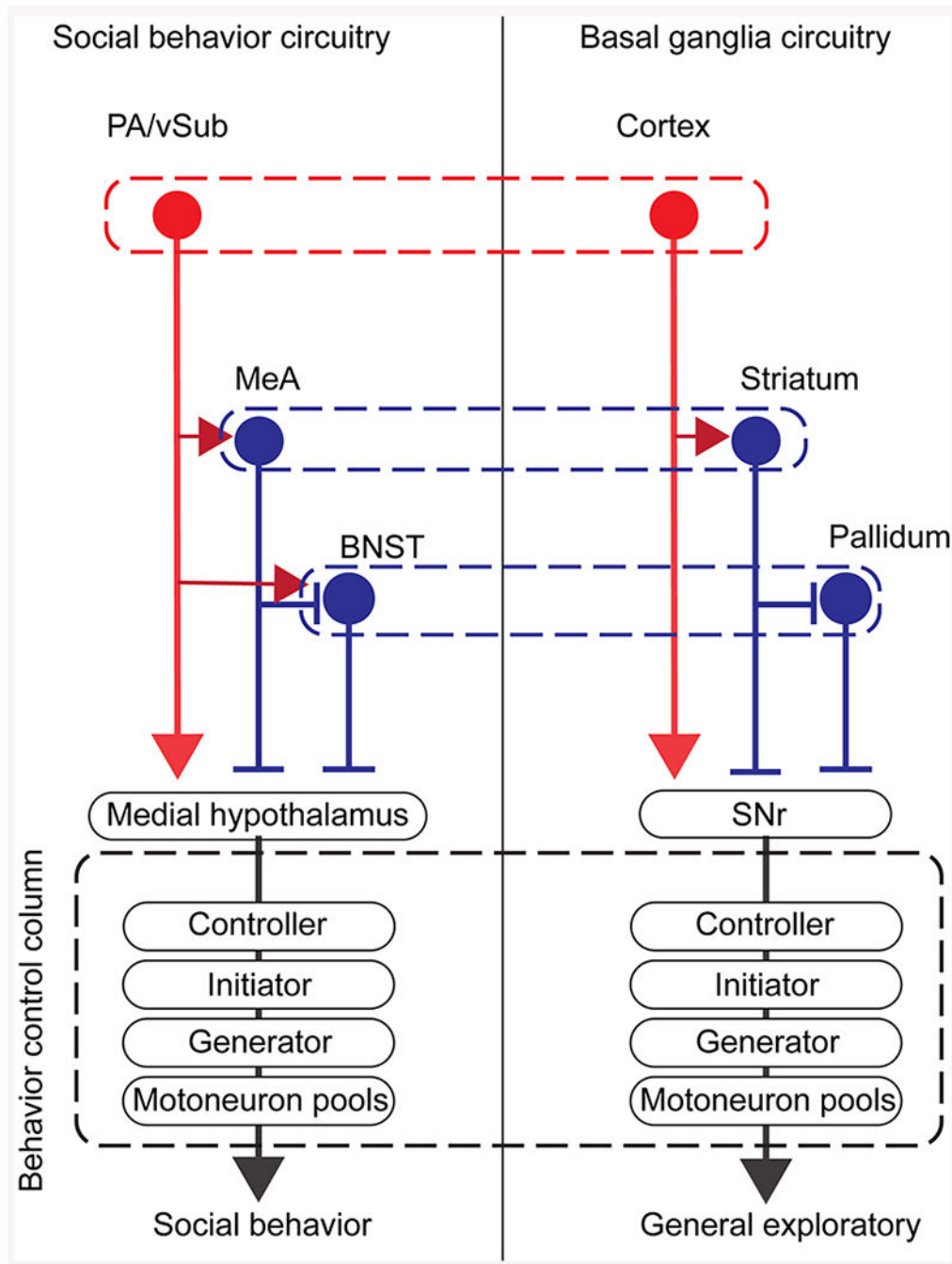
latency to attempted mount, shallow thrust and increased the duration of attempted mount and shallow thrust while only 0.5 mg/kg promoted female-directed aggression. (**h-m**) CNO injection into PA<sup>Esr1+MPN</sup> hM3Dq expressing animals did not promote male-directed aggression regardless of the CNO concentration. (**n**) Representative raster plots showing the behaviors towards male and female intruders after saline, 0.1 mg/kg CNO and 0.5 mg/kg CNO i.p. injection in PA<sup>Esr1+VMHvl</sup> hM3Dq expressing animals. Scale bar: 60 s. (**o-z**) 0.5 mg/kg CNO i.p. injection in PA<sup>Esr1+VMHvl</sup> hM3Dq expressing animals caused a significant decrease in attack latency (**s** and **y**) and an increase in attack duration (**t** and **z**) towards both male and female intruders. Animals with 0.1 mg/kg CNO showed an increased trend of attack. Each test lasts 10 minutes. For animals that did not show the relevant behaviors within the testing period, the latency will be set at 600 s. n = 8 animals in **b-m** and **o-z**. All data in **b-m** and **o-z** are presented as mean ± s.e.m. Repeated measure One-way ANOVA with Geisser-Greenhouse's correction followed by Tukey's multiple comparison test in **p**; Friedman test followed by Dann's multiple comparisons test in **b-g**, **l-o** and **q-z**. \*p < 0.05; \*\*p < 0.01. Brain atlas images in **a** are modified from<sup>51</sup>. For detailed statistics information, see Supplementary Table 1.



**Extended Data Fig. 9. Optogenetic activation of  $PA^{Esr1+VMHvl}$  neurons promotes aggression while optogenetic activating  $PA^{Esr1+MPN}$  cells fails to cause behavioral change in naïve male mice, related to Figure 6.**

(a) Experimental schematics. (b) Representative images showing the expressions of ChR2-EYFP (green) and DAPI (blue) in  $PA^{Esr1+MPN}$  (top) and  $PA^{Esr1+VMHvl}$  (bottom) cells. Scale bar: 200 μm. Dashed lines outline the PA. Solid white lines indicate the placement of optic fibers. (c) Test schedule. (d and e) Representative raster plots illustrating behaviors against various intruders during and between light stimulation. Scale bar: 60 s. Top showing light-on period in cyan. Bottom showing behaviors. (f-j) Optogenetic activation of  $PA^{Esr1+MPN}$  cells

did not cause any measurable change in sexual and aggressive behaviors towards any intruder. **(k-o)** The percentage of trials that animals attacked (**k**), average latency to attack during each trial (**l**), and the average duration of attack per trial (**m**) towards male intruder, but not castrated male and female intruder, increased with light stimulation. **(n and o)** Light stimulation did not change duration of sniffing (**n**) or mounting (**o**) towards any intruders. **(p-t)** Animals expressing EYFP in PA<sup>Esr1+VMHvl</sup> neurons showed no behavioral changes during light stimulation. n = 5 animals for each group. All data in **f-t** shown as mean ± s.e.m. Two-tailed paired *t*-test (**i, k, l, m, n, s** and **t**) and Wilcoxon matched-pairs signed rank test (**g, h, j, l, o-t**). \*p < 0.05. For detailed statistics information, see Supplementary Table 1.



**Extended Data Fig. 10. A basic wiring diagram showing triple descending projections from the cerebral hemisphere to the behavior control column that drives social behaviors and general exploration, related to Figures 1, 7.**

In parallel to the classical cortico-striato-nigral circuit that controls general exploration, PA/vSub (cortex equivalent), MeA (striatum equivalent) and BNST (pallidum equivalent) modulate the rostral part of the behavior control column (including MPN and VMHvI) through triple descending projections – a cortical excitatory projection, a striatal inhibitory projection and a pallidal disinhibitory projection. SNr: substantia nigra pars reticulata.

## Supplementary Material

Refer to Web version on PubMed Central for supplementary material.

## Acknowledgements

We thank C. Loomis at the NYULMC Experimental Pathology Research Laboratory for help on laser capture microdissection, A. Heguy and Y. Zhang at the NYULMC Genome Technology Center for help on RNA-seq and V. Varshini at the NYULMC Bioinformatics Laboratory for help with sequence alignment. This research was supported by a JSPS oversea fellowship (T.Y.); a Uehara postdoctoral fellowship (T.Y.); NIH R01MH107742 and R01MH108594 (B.L.), NIH R00NS087098 and DP2NS105553 (N.X.T.); the Leon Levy Foundation (N.X.T.); the Dana Foundation (N.X.T.); the Alfred P. Sloan Foundation (N.X.T. and D.L.); the Whitehall Foundations (N.X.T. and D.L.); NIH R01MH101377, R21MH105774, 1R01HD092596, U19NS107616 (D.L.); the Mathers Foundation (D.L.); an Irma T. Hirschl Career Scientist Award (D.L.); and a McKnight Scholar Award (D.L.).

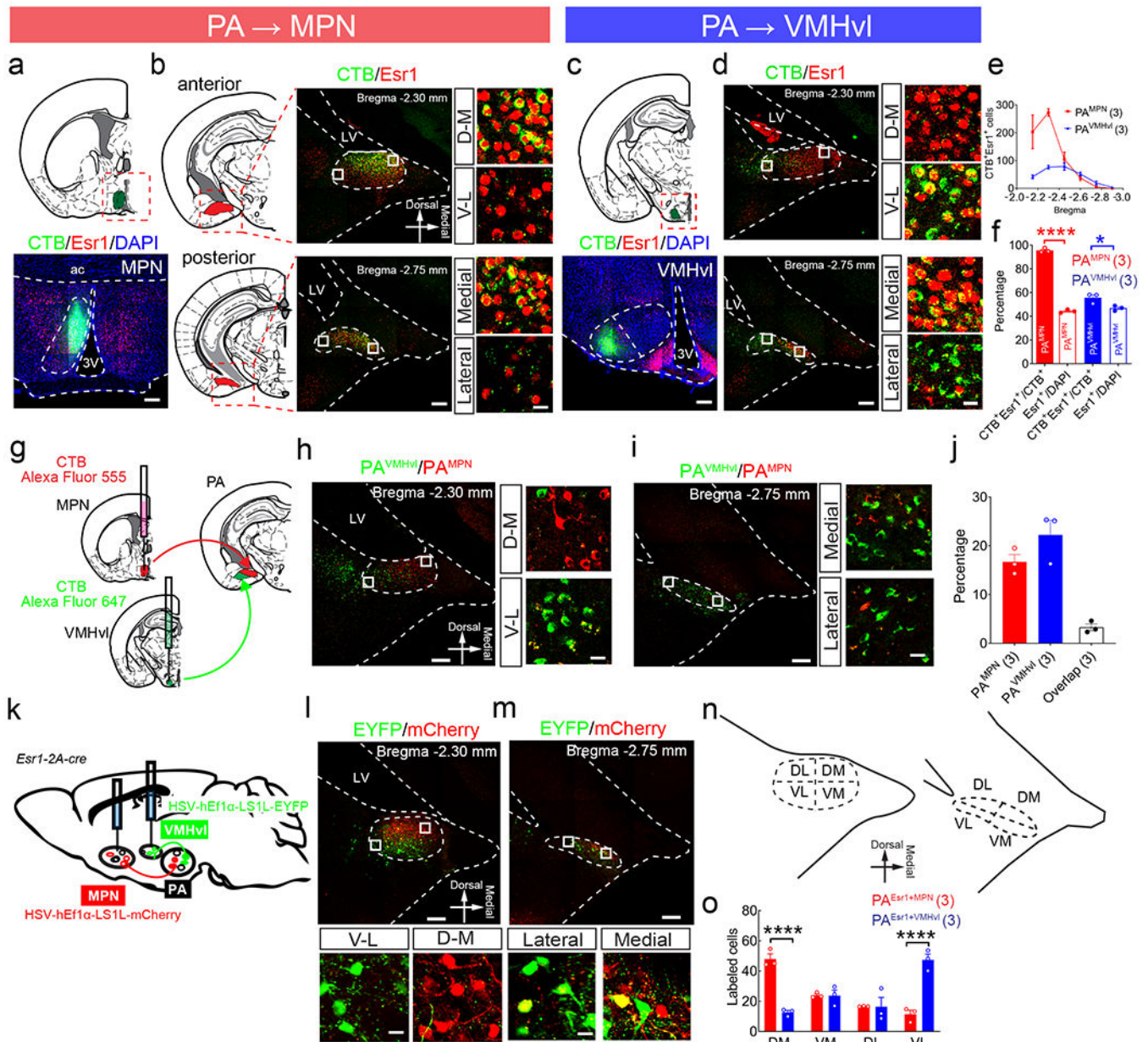
## References

1. Coolen LM & Wood RI Testosterone stimulation of the medial preoptic area and medial amygdala in the control of male hamster sexual behavior: redundancy without amplification. *Behav Brain Res* 98, 143–153, doi:10.1016/s0166-4328(98)00063-1 (1999). [PubMed: 10210530]
2. Arendash GW & Gorski RA Effects of discrete lesions of the sexually dimorphic nucleus of the preoptic area or other medial preoptic regions on the sexual behavior of male rats. *Brain Res Bull* 10, 147–154, doi:10.1016/0361-9230(83)90086-2 (1983). [PubMed: 6824962]
3. Klaric JS & Hendricks SE Effects of two-stage lesions of the medial preoptic area on sexual behavior of male rats. *Physiol Behav* 37, 539–542, doi:10.1016/0031-9384(86)90281-7 (1986). [PubMed: 3749316]
4. Malsbury CW Facilitation of male rat copulatory behavior by electrical stimulation of the medial preoptic area. *Physiol Behav* 7, 797–805, doi:10.1016/0031-9384(71)90042-4 (1971). [PubMed: 5134017]
5. Wei YC et al. Medial preoptic area in mice is capable of mediating sexually dimorphic behaviors regardless of gender. *Nat Commun* 9, 279, doi:10.1038/s41467-017-02648-0 (2018). [PubMed: 29348568]
6. Lin D et al. Functional identification of an aggression locus in the mouse hypothalamus. *Nature* 470, 221–226, doi:10.1038/nature09736 (2011). [PubMed: 21307935]
7. Lee H et al. Scalable control of mounting and attack by *Esr1*+ neurons in the ventromedial hypothalamus. *Nature* 509, 627–632, doi:10.1038/nature13169 (2014). [PubMed: 24739975]
8. Yang CF et al. Sexually dimorphic neurons in the ventromedial hypothalamus govern mating in both sexes and aggression in males. *Cell* 153, 896–909, doi:10.1016/j.cell.2013.04.017 (2013). [PubMed: 23663785]
9. Yang T et al. Social Control of Hypothalamus-Mediated Male Aggression. *Neuron*, doi:10.1016/j.neuron.2017.06.046 (2017).
10. Falkner AL, Grosenick L, Davidson TJ, Deisseroth K & Lin D Hypothalamic control of male aggression-seeking behavior. *Nature neuroscience* 19, 596 (2016). [PubMed: 26950005]
11. Wang L et al. Hypothalamic control of conspecific self-defense. *Cell reports* 26, 1747–1758. e1745 (2019). [PubMed: 30759387]
12. Stagkourakis S et al. A neural network for intermale aggression to establish social hierarchy. *Nat Neurosci* 21, 834–842, doi:10.1038/s41593-018-0153-x (2018). [PubMed: 29802391]
13. Bergan JF, Ben-Shaul Y & Dulac C Sex-specific processing of social cues in the medial amygdala. *Elife* 3, e02743, doi:10.7554/eLife.02743 (2014). [PubMed: 24894465]
14. Hong W, Kim DW & Anderson DJ Antagonistic control of social versus repetitive self-grooming behaviors by separable amygdala neuronal subsets. *Cell* 158, 1348–1361, doi:10.1016/j.cell.2014.07.049 (2014). [PubMed: 25215491]
15. Lehman MN, Winans SS & Powers JB Medial nucleus of the amygdala mediates chemosensory control of male hamster sexual behavior. *Science* 210, 557–560, doi:10.1126/science.7423209 (1980). [PubMed: 7423209]

16. Li Y et al. Neuronal Representation of Social Information in the Medial Amygdala of Awake Behaving Mice. *Cell* 171, 1176–1190 e1117, doi:10.1016/j.cell.2017.10.015 (2017). [PubMed: 29107332]
17. Unger EK et al. Medial amygdalar aromatase neurons regulate aggression in both sexes. *Cell Rep* 10, 453–462, doi:10.1016/j.celrep.2014.12.040 (2015). [PubMed: 25620703]
18. Miller SM, Marcotulli D, Shen A & Zweifel LS Divergent medial amygdala projections regulate approach-avoidance conflict behavior. *Nat Neurosci* 22, 565–575, doi:10.1038/s41593-019-0337-z (2019). [PubMed: 30804529]
19. Dulac C & Wagner S Genetic analysis of brain circuits underlying pheromone signaling. *Annu Rev Genet* 40, 449–467, doi:10.1146/annurev.genet.39.073003.093937 (2006). [PubMed: 16953793]
20. Coolen LM, Peters HJ & Veening JG Distribution of Fos immunoreactivity following mating versus anogenital investigation in the male rat brain. *Neuroscience* 77, 1151–1161, doi:10.1016/s0306-4522(96)00542-8 (1997). [PubMed: 9130794]
21. Kim Y et al. Mapping social behavior-induced brain activation at cellular resolution in the mouse. *Cell Rep* 10, 292–305, doi:10.1016/j.celrep.2014.12.014 (2015). [PubMed: 25558063]
22. Dong HW & Swanson LW Projections from bed nuclei of the stria terminalis, posterior division: implications for cerebral hemisphere regulation of defensive and reproductive behaviors. *J Comp Neurol* 471, 396–433, doi:10.1002/cne.20002 (2004). [PubMed: 15022261]
23. Bayless DW et al. Limbic Neurons Shape Sex Recognition and Social Behavior in Sexually Naive Males. *Cell* 176, 1190–1205 e1120, doi:10.1016/j.cell.2018.12.041 (2019). [PubMed: 30712868]
24. Brody J, DeFeudis P & DeFeudis FJN Effects of micro-injections of L-glutamate into the hypothalamus on attack and flight behaviour in cats. *Nature* 224, 1330–1330 (1969). [PubMed: 5391022]
25. Dominguez JM, Gil M & Hull EM Preoptic glutamate facilitates male sexual behavior. *J Neurosci* 26, 1699–1703, doi:10.1523/JNEUROSCI.4176-05.2006 (2006). [PubMed: 16467517]
26. Canteras NS, Simerly RB & Swanson LW Connections of the posterior nucleus of the amygdala. *J Comp Neurol* 324, 143–179, doi:10.1002/cne.903240203 (1992). [PubMed: 1430327]
27. Watson C, Paxinos G & Puelles L The mouse nervous system. 1st edn, 140–72 (Elsevier Academic Press, 2012).
28. Simerly RB Wired for reproduction: organization and development of sexually dimorphic circuits in the mammalian forebrain. *Annu Rev Neurosci* 25, 507–536, doi:10.1146/annurev.neuro.25.112701.142745 (2002). [PubMed: 12052919]
29. Fang YY, Yamaguchi T, Song SC, Tritsch NX & Lin D A Hypothalamic Midbrain Pathway Essential for Driving Maternal Behaviors. *Neuron* 98, 192–207 e110, doi:10.1016/j.neuron.2018.02.019 (2018). [PubMed: 29621487]
30. Hashikawa K et al. Esr1(+) cells in the ventromedial hypothalamus control female aggression. *Nat Neurosci* 20, 1580–1590, doi:10.1038/nn.4644 (2017). [PubMed: 28920934]
31. Simerly RB, Chang C, Muramatsu M & Swanson LW Distribution of androgen and estrogen receptor mRNA-containing cells in the rat brain: an in situ hybridization study. *J Comp Neurol* 294, 76–95, doi:10.1002/cne.902940107 (1990). [PubMed: 2324335]
32. Ervin KS et al. Estrogen involvement in social behavior in rodents: Rapid and long-term actions. *Horm Behav* 74, 53–76, doi:10.1016/j.yhbeh.2015.05.023 (2015). [PubMed: 26122289]
33. Kollack-Walker S & Newman SW Mating and agonistic behavior produce different patterns of Fos immunolabeling in the male Syrian hamster brain. *Neuroscience* 66, 721–736, doi:10.1016/0306-4522(94)00563-k (1995). [PubMed: 7644033]
34. Swanson LW Cerebral hemisphere regulation of motivated behavior. *Brain Res* 886, 113–164, doi:10.1016/s0006-8993(00)02905-x (2000). [PubMed: 11119693]
35. Wang L et al. Hypothalamic Control of Conspecific Self-Defense. *Cell Rep* 26, 1747–1758 e1745, doi:10.1016/j.celrep.2019.01.078 (2019). [PubMed: 30759387]
36. Wang F et al. RNAscope: a novel in situ RNA analysis platform for formalin-fixed, paraffin-embedded tissues. *J Mol Diagn* 14, 22–29, doi:10.1016/j.jmoldx.2011.08.002 (2012). [PubMed: 22166544]
37. Gunaydin LA et al. Natural neural projection dynamics underlying social behavior. *Cell* 157, 1535–1551, doi:10.1016/j.cell.2014.05.017 (2014). [PubMed: 24949967]

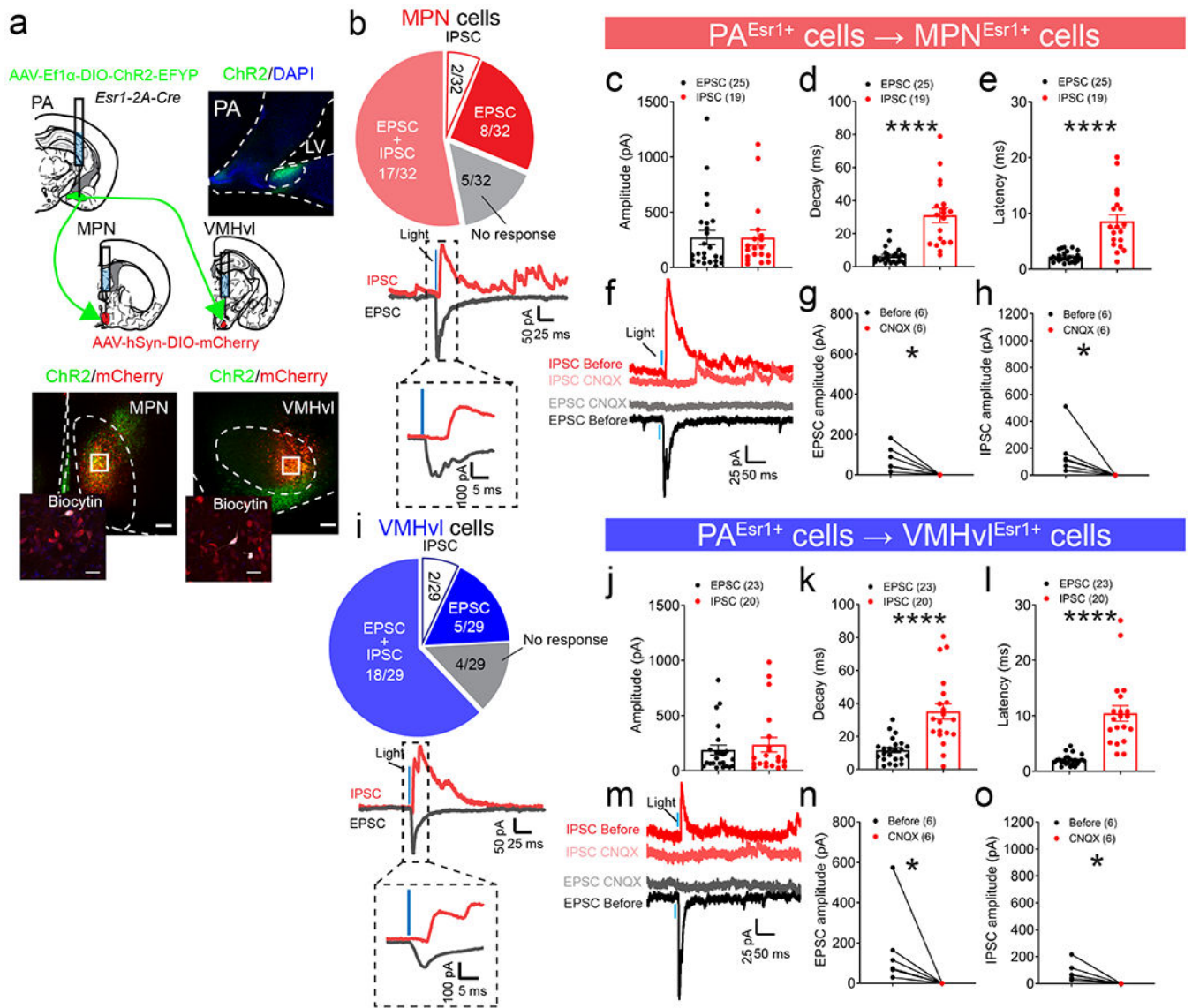
38. Cui G et al. Concurrent activation of striatal direct and indirect pathways during action initiation. *Nature* 494, 238–242, doi:nature11846 [pii] 10.1038/nature11846 (2013). [PubMed: 23354054]
39. Knowland D et al. Distinct Ventral Pallidal Neural Populations Mediate Separate Symptoms of Depression. *Cell* 170, 284–297 e218, doi:10.1016/j.cell.2017.06.015 (2017). [PubMed: 28689640]
40. Alexander GM et al. Remote control of neuronal activity in transgenic mice expressing evolved G protein-coupled receptors. *Neuron* 63, 27–39, doi:10.1016/j.neuron.2009.06.014 (2009). [PubMed: 19607790]
41. Schwarz LA et al. Viral-genetic tracing of the input-output organization of a central noradrenergic circuit. *Nature* 524, 88–92, doi:10.1038/nature14600 (2015). [PubMed: 26131933]
42. Canteras NS, Simerly RB & Swanson LW Organization of projections from the medial nucleus of the amygdala: a PHAL study in the rat. *J Comp Neurol* 360, 213–245, doi:10.1002/cne.903600203 (1995). [PubMed: 8522644]
43. Petrovich GD, Canteras NS & Swanson LW Combinatorial amygdalar inputs to hippocampal domains and hypothalamic behavior systems. *Brain Res Brain Res Rev* 38, 247–289 (2001). [PubMed: 11750934]
44. Zha X et al. VMHvl-Projecting Vglut1+ Neurons in the Posterior Amygdala Gate Territorial Aggression. *Cell Rep* 31, 107517, doi:10.1016/j.celrep.2020.03.081 (2020). [PubMed: 32320666]
45. Emery DE & Sachs BD Copulatory behavior in male rats with lesions in the bed nucleus of the stria terminalis. *Physiol Behav* 17, 803–806, doi:10.1016/0031-9384(76)90044-5 (1976). [PubMed: 1026988]
46. Liu YC, Salamone JD & Sachs BD Lesions in medial preoptic area and bed nucleus of stria terminalis: differential effects on copulatory behavior and noncontact erection in male rats. *J Neurosci* 17, 5245–5253 (1997). [PubMed: 9185562]
47. Shimura T, Yamamoto T & Shimokochi M The medial preoptic area is involved in both sexual arousal and performance in male rats: re-evaluation of neuron activity in freely moving animals. *Brain Res* 640, 215–222, doi:10.1016/0006-8993(94)91875-9 (1994). [PubMed: 8004448]
48. Hoffman NW, Kim YI, Gorski RA & Dudek FE Homogeneity of intracellular electrophysiological properties in different neuronal subtypes in medial preoptic slices containing the sexually dimorphic nucleus of the rat. *J Comp Neurol* 345, 396–408, doi:10.1002/cne.903450306 (1994). [PubMed: 7929908]
49. Hatayama M et al. Zic2 hypomorphic mutant mice as a schizophrenia model and ZIC2 mutations identified in schizophrenia patients. *Sci Rep* 1, 16, doi:10.1038/srep00016 (2011). [PubMed: 22355535]
50. Lewis AS et al. Bidirectional Regulation of Aggression in Mice by Hippocampal Alpha-7 Nicotinic Acetylcholine Receptors. *Neuropsychopharmacology* 43, 1267–1275, doi:10.1038/npp.2017.276 (2018). [PubMed: 29114104]
51. Paxinos G & Franklin KBJ The mouse brain in stereotaxic coordinates. 3rd edn. (Elsevier Academic Press, 2008).
52. Vong L et al. Leptin action on GABAergic neurons prevents obesity and reduces inhibitory tone to POMC neurons. *Neuron* 71, 142–154, doi:10.1016/j.neuron.2011.05.028 (2011). [PubMed: 21745644]
53. Madisen L et al. A robust and high-throughput Cre reporting and characterization system for the whole mouse brain. *Nat Neurosci* 13, 133–140, doi:10.1038/nn.2467 (2010). [PubMed: 20023653]
54. Yamaguchi T, Danjo T, Pastan I, Hikida T & Nakanishi S Distinct roles of segregated transmission of the septo-habenular pathway in anxiety and fear. *Neuron* 78, 537–544, doi:10.1016/j.neuron.2013.02.035 (2013). [PubMed: 23602500]
55. Mathis A et al. DeepLabCut: markerless pose estimation of user-defined body parts with deep learning. *Nat Neurosci* 21, 1281–1289, doi:10.1038/s41593-018-0209-y (2018). [PubMed: 30127430]
56. Nilsson SR et al. Simple Behavioral Analysis (SimBA) – an open source toolkit for computer classification of complex social behaviors in experimental animals. 2020.2004.2019.049452, doi:10.1101/2020.04.19.049452 %J bioRxiv (2020).

57. Wang L, Chen IZ & Lin D Collateral pathways from the ventromedial hypothalamus mediate defensive behaviors. *Neuron* 85, 1344–1358, doi:10.1016/j.neuron.2014.12.025 (2015). [PubMed: 25754823]
58. Dobin A et al. STAR: ultrafast universal RNA-seq aligner. *Bioinformatics* 29, 15–21, doi:10.1093/bioinformatics/bts635 (2013). [PubMed: 23104886]
59. Cimmino L et al. Restoration of TET2 Function Blocks Aberrant Self-Renewal and Leukemia Progression. *Cell* 170, 1079–1095 e1020, doi:10.1016/j.cell.2017.07.032 (2017). [PubMed: 28823558]
60. Liao Y, Smyth GK & Shi W featureCounts: an efficient general purpose program for assigning sequence reads to genomic features. *Bioinformatics* 30, 923–930, doi:10.1093/bioinformatics/btt656 (2014). [PubMed: 24227677]
61. Ritchie ME et al. limma powers differential expression analyses for RNA-sequencing and microarray studies. *Nucleic Acids Res* 43, e47, doi:10.1093/nar/gkv007 (2015). [PubMed: 25605792]
62. Ge SX, Son EW & Yao R iDEP: an integrated web application for differential expression and pathway analysis of RNA-Seq data. *BMC Bioinformatics* 19, 534, doi:10.1186/s12859-018-2486-6 (2018). [PubMed: 30567491]



**Figure 1. Largely distinct subpopulations of PA<sup>Esr1+</sup> neurons project to the MPN and VMHvl** (a and c) Examples showing CTB injection sites (green) in the MPN and VMHvl. Scale bars: 200  $\mu$ m. (b and d) Representative images showing Esr1 expression (red) and CTB labeling (green) in the anterior (top row, Bregma level: -2.30 mm) and posterior (bottom row, Bregma: -2.75 mm) parts of the PA after CTB injections into the MPN (a) and VMHvl (b). Right showing magnified views of the white boxed areas. Scale bars: 200  $\mu$ m (left) and 20  $\mu$ m (right). (e) The number of CTB<sup>+</sup> cells along the anterior-posterior axis of PA after CTB injections into the MPN (red line) and VMHvl (blue line). (f) The percentage of CTB<sup>+</sup> cells expressing Esr1 and the percentage of Esr1<sup>+</sup> cells in the PA total population. In e and f, n = 3 VMHvl-injected animals and 3 MPN-injected animals. Two-tailed unpaired t-test. \* $p$  < 0.05, \*\*\*\* $p$  < 0.0001. (g) Experimental Schematics for dual labeling of PA<sup>MPN</sup> and PA<sup>VMHvl</sup>. (h and i) Representative images showing PA<sup>VMHvl</sup>/PA<sup>MPN</sup> dual labeling. Scale bars: 200  $\mu$ m (left) and 20  $\mu$ m (right). (j) The percentage of PA<sup>MPN</sup>, PA<sup>VMHvl</sup>, and Overlap cells. (k) Esr1-2A-cre mouse model and HSV-hE1 $\alpha$ -LS1L-mCherry injection site. (l and m) Representative images showing EYFP/mCherry dual labeling. Scale bars: 200  $\mu$ m (left) and 20  $\mu$ m (right). (n) Schematic diagrams of the PA subregions (DL, DM, VL, VM). (o) The number of labeled cells in each subregion. \*\*\*\* $p$  < 0.0001.

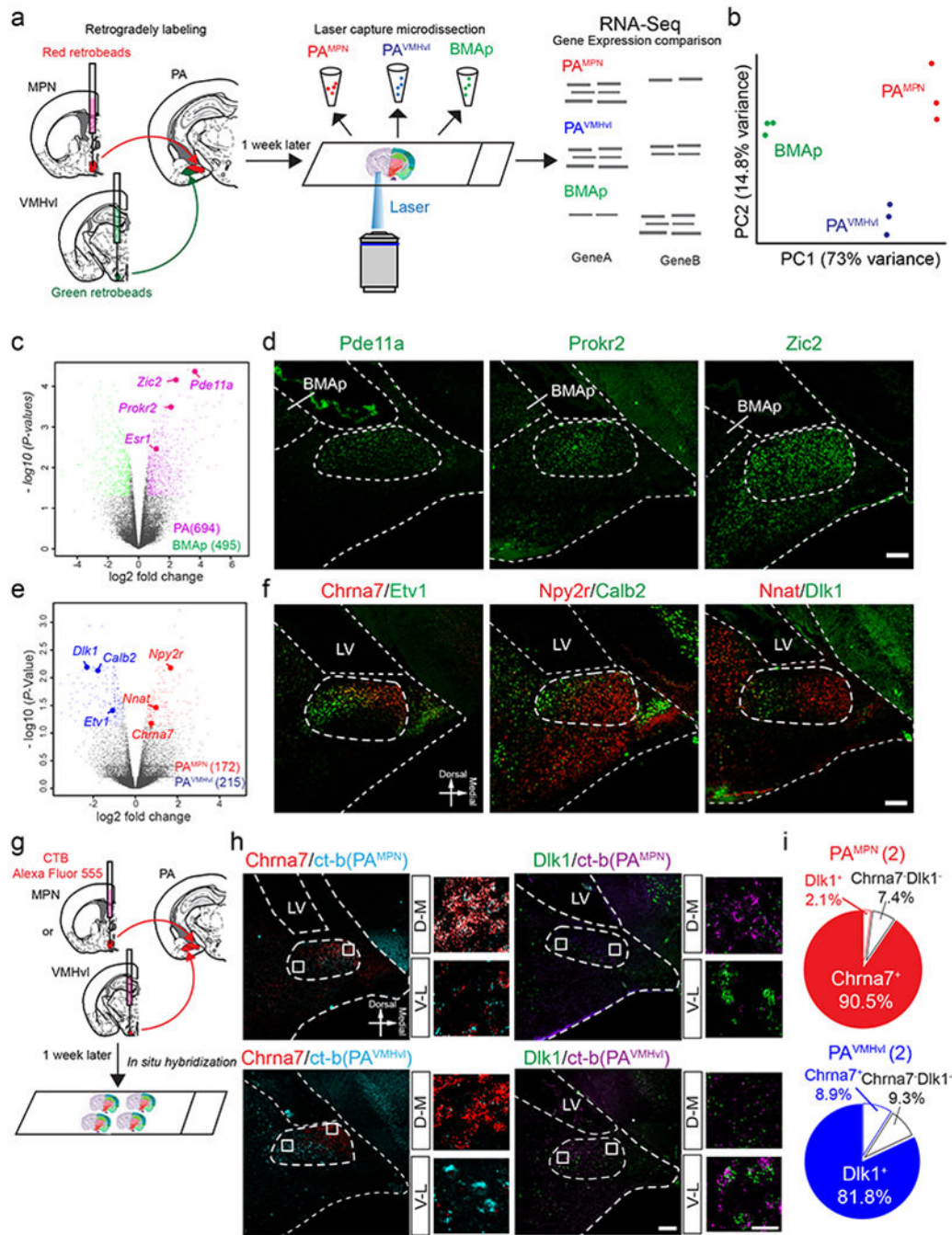
PA<sup>VMHvl</sup> cells with Alexa555-CTB and Alexa647-CTB. **(h and i)** Representative images showing MPN- (red) and VMHvl-projecting (green) cells in the anterior **(h)** and posterior parts of the PA **(i)**. Right showing magnified views of the white boxed areas on the left. Scale bars: 200  $\mu$ m (left) and 20  $\mu$ m (right). **(j)** The percentage of CTB<sup>+</sup> and overlapping cells in the PA total population. n = 3 animals. **(k)** Viral strategy for dual-retrograde labeling of PA<sup>Esr1+MPN</sup> and PA<sup>Esr1+VMHvl</sup> cells. **(l and m)** Representative images showing EYFP (green, from VMHvl) and mCherry (red, from MPN) labeled cells in the anterior **(l)** and posterior parts of PA **(m)**. Bottom showing magnified views of the white boxed areas. Scale bars: 200  $\mu$ m (top) and 20  $\mu$ m (bottom). **(n)** Schematics showing the four subregions in the anterior (left) and posterior (right) PA where the cell counts are obtained. **(o)** The number of retrogradely labeled PA<sup>Esr1+MPN</sup> and PA<sup>Esr1+VMHvl</sup> cells in each of the four subregions across the anterior and posterior PA. n = 3 animals. Images in **a-d, h, i, l** and **m** are representative of n = 3 mice. Two-way ANOVA with Bonferroni's multiple comparison test. \*\*\*\*p < 0.0001. All data in **e, f, j**, and **o** are expressed as mean  $\pm$  s.e.m. Brain atlas images in **a-c** and **g** are modified from<sup>51</sup>. See also Extended Data Fig. 1, 10. For detailed statistics information, see Supplementary Table 1.



**Figure 2.** PA<sup>Esr1+</sup> cells provides monosynaptic excitatory inputs to MPN<sup>Esr1+</sup> and VMHvl<sup>Esr1+</sup> cells.

(a) Schematics for the channelrhodopsin assisted circuit mapping and example image showing ChR2-EYFP expression in PA<sup>Esr1+</sup> cells (upper right), ChR2-EYFP fibers from PA and mCherry<sup>+</sup> cells in MPN (bottom left) and VMHvl (bottom right). Insets show magnified views of the white boxes that contain mCherry expressing cells (red) and biocytin filled recorded cells (white). Scale bars: 200 μm (top) and 20 μm (insets). Brain atlas images are modified from<sup>51</sup>. Histological images are representative of n = 10 animals. (b and i) Pie charts showing light-evoked synaptic responses in MPN<sup>Esr1+</sup> (b) and VMHvl<sup>Esr1+</sup> cells (i). Bottom showing example EPSC and IPSC traces evoked by 0.5-ms blue light pulses and the expanded views of the boxed areas. Blue vertical lines indicate light pulses. (c - e) The amplitude (c), decay time (d), and latency (e) of light-evoked EPSCs (left) and IPSCs (right) of MPN<sup>Esr1+</sup> cells. n = 25 and 19 cells from 10 animals. (f) The example light evoked EPSC and IPSC traces before and after CNQX bath application. n = 6 cells from 6 animals. (g and

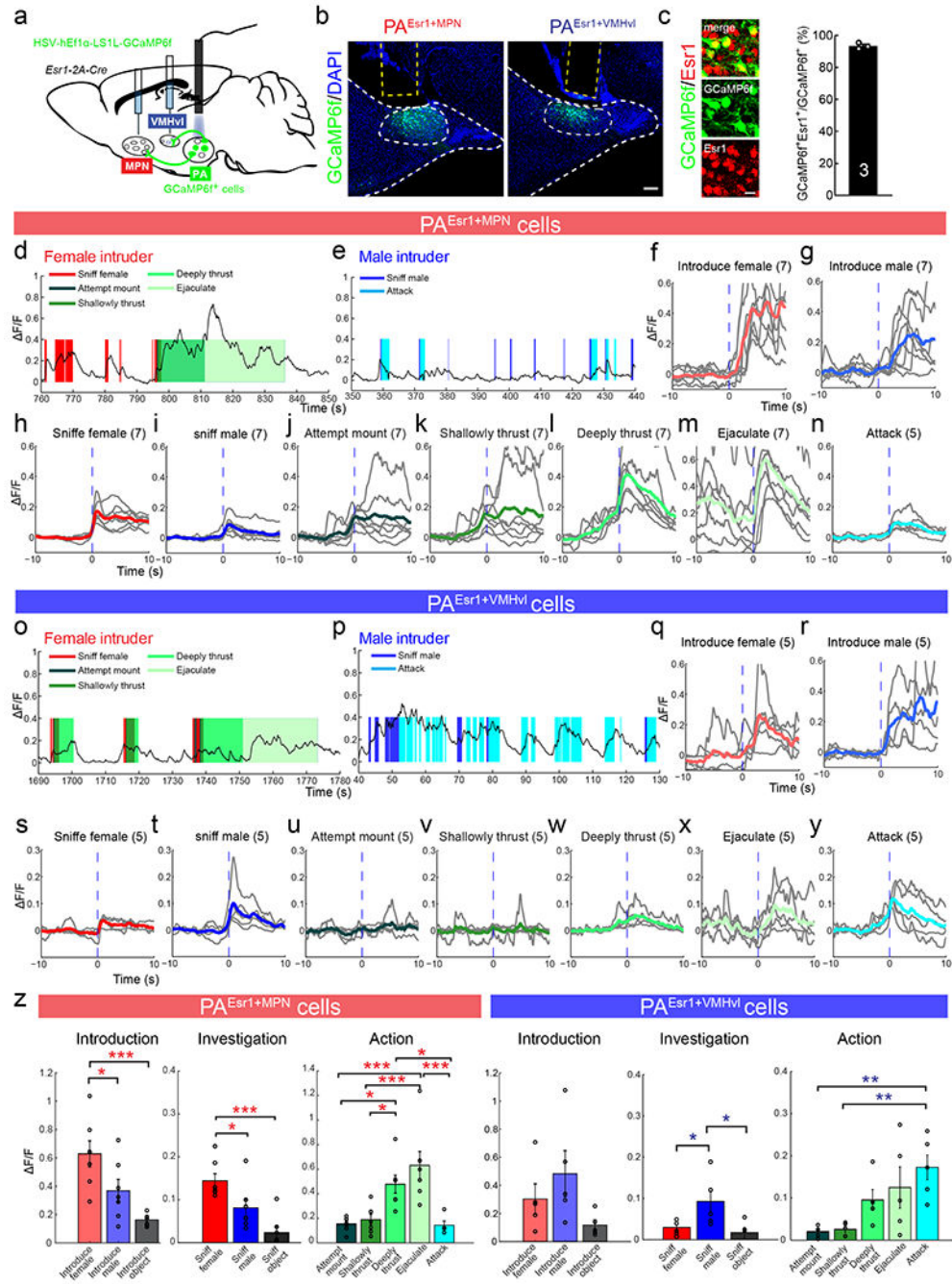
**h)** The light-evoked EPSCs (**g**) and IPSCs (**h**) are abolished after bath application of CNQX.  $n = 6$  cells from 6 animals. (**j - o**) Characterization of light-evoked EPSCs and IPSCs in the VMHv1<sup>Esr1+</sup> cells.  $n = 23$  and 20 cells from in 10 animals in **j - l**.  $n = 6$  cells from 6 animals in **n** and **o**. All data in **c-e** and **j-l** are presented as mean  $\pm$  s.e.m. Two-tailed unpaired t-test (**e** and **k**), Mann Whitney test (**c, d, j** and **l**) and Wilcoxon matched-pairs signed rank test (**g, h, n** and **o**). \* $p < 0.05$ , \*\*\*\* $p < 0.0001$ . See also Extended Data Fig. 2. For detailed statistics information, see Supplementary Table 1.



**Figure 3. Largely distinct transcriptional profiles for PA subregions projecting to MPN and VMHvl.**

(a) Experimental schematics. (b) Map the RNA-seq results of all samples onto the principal component (PC) space. Note that samples from the same PA subregion are clustered and separated from the other neighboring areas. (c) A volcano plot illustrating genes enriched in the BMAp (green dots BMAp/PA > 1.5,  $p < 0.05$ ) and PA (magenta dots, PA/BMAp > 1.5,  $p < 0.05$ ). Gray dots denote genes with  $p \geq 0.05$  or fold enrichment  $\leq 1.5$  based on the limma method.  $n = 3$  animals. (d) RNA expression patterns of three PA enriched genes:

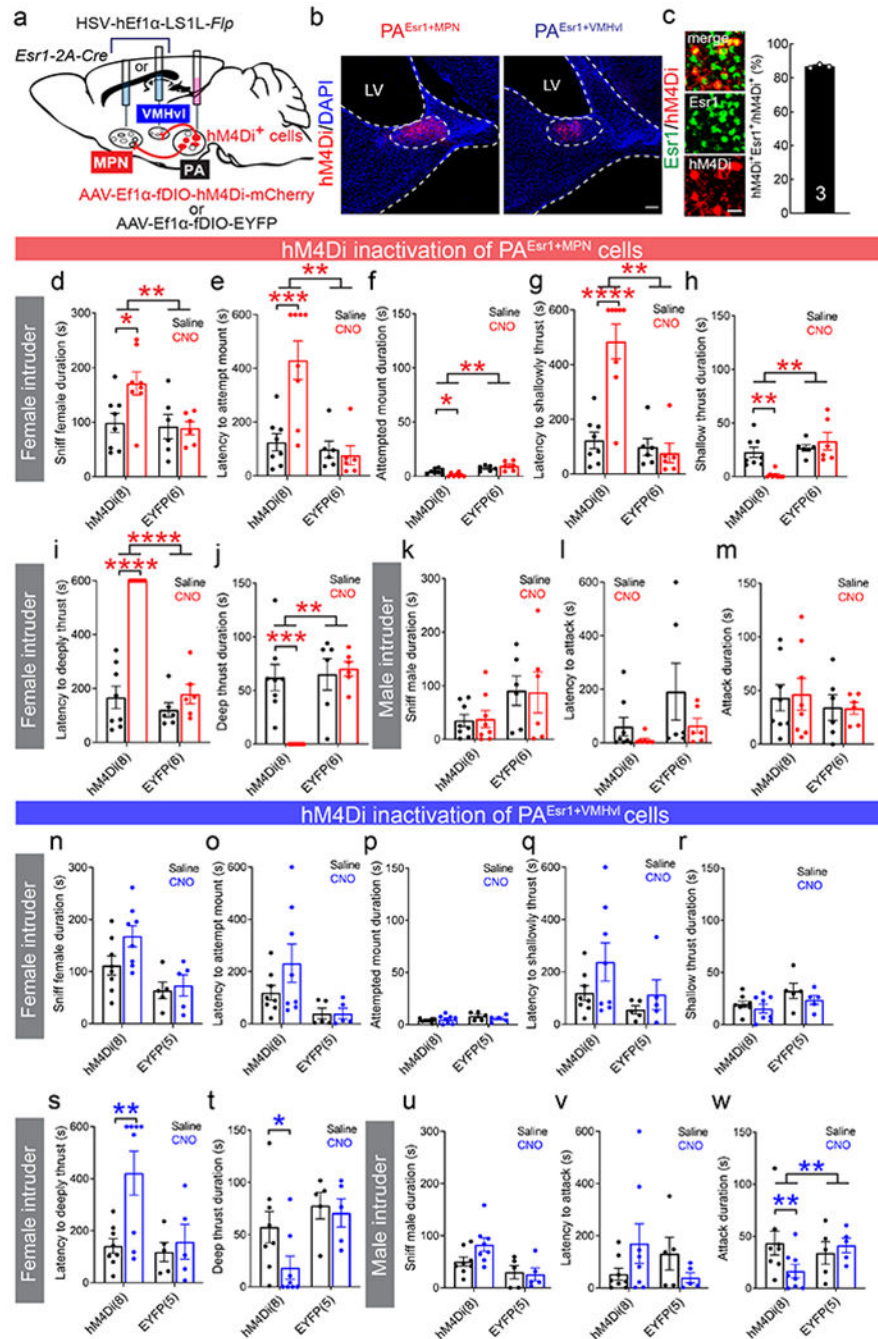
*Pde11a*, *Prokr2* and *Zic2*. Scale bar: 200  $\mu\text{m}$ . (e) A volcano plot illustrating genes enriched in PA<sup>VMHvl</sup> (blue dots,  $\text{PA}^{\text{VMHvl}}/\text{PA}^{\text{MPN}} > 1.5$ ,  $p < 0.07$ ) and PA<sup>MPN</sup> (red dots,  $\text{PA}^{\text{MPN}}/\text{PA}^{\text{VMHvl}} > 1.5$ ,  $p < 0.07$ ). Gray dots denote genes that commonly express in PA<sup>MPN</sup> and PA<sup>VMHvl</sup> based on the limma method.  $n = 3$  animals. (f) RNA expression patterns of PA<sup>MPN</sup> and PA<sup>VMHvl</sup> enriched genes as indicated in (e). Scale bar: 200  $\mu\text{m}$ . (g) Experimental Schematics for labeling PA<sup>MPN</sup> or PA<sup>VMHvl</sup> cells and examining their overlap with specific genes. (h) Example images of PA<sup>MPN</sup> and PA<sup>VMHvl</sup> cells labeled with Alexa555-CTB and the RNA expression pattern of *Chrna7* and *Dlk1*. *Chrna7* overlaps with PA<sup>MPN</sup> but not PA<sup>VMHvl</sup> cells while *Dlk1* overlaps with PA<sup>VMHvl</sup> but not PA<sup>MPN</sup> cells. Right showing the enlarged views of the boxed areas. Scale bars: 200  $\mu\text{m}$  (left) and 20  $\mu\text{m}$  (right). (i) Pie charts showing the percentage of PA<sup>MPN</sup> cells (top) and PA<sup>VMHvl</sup> cells (bottom) that express *Chrna7*, *Dlk1* or neither.  $n = 2$  animals. Empirical Bayes moderated two-tailed *t*-test with Benjamini-Hochberg procedure based on the limma method (c and e). Brain atlas images in a and g are modified from<sup>51</sup>. For detailed statistics information, see Supplementary Table 1.



**Figure 4. Different response patterns of PA<sup>Esr1+MPN</sup> and PA<sup>Esr1+VMHvl</sup> cells during social behaviors**

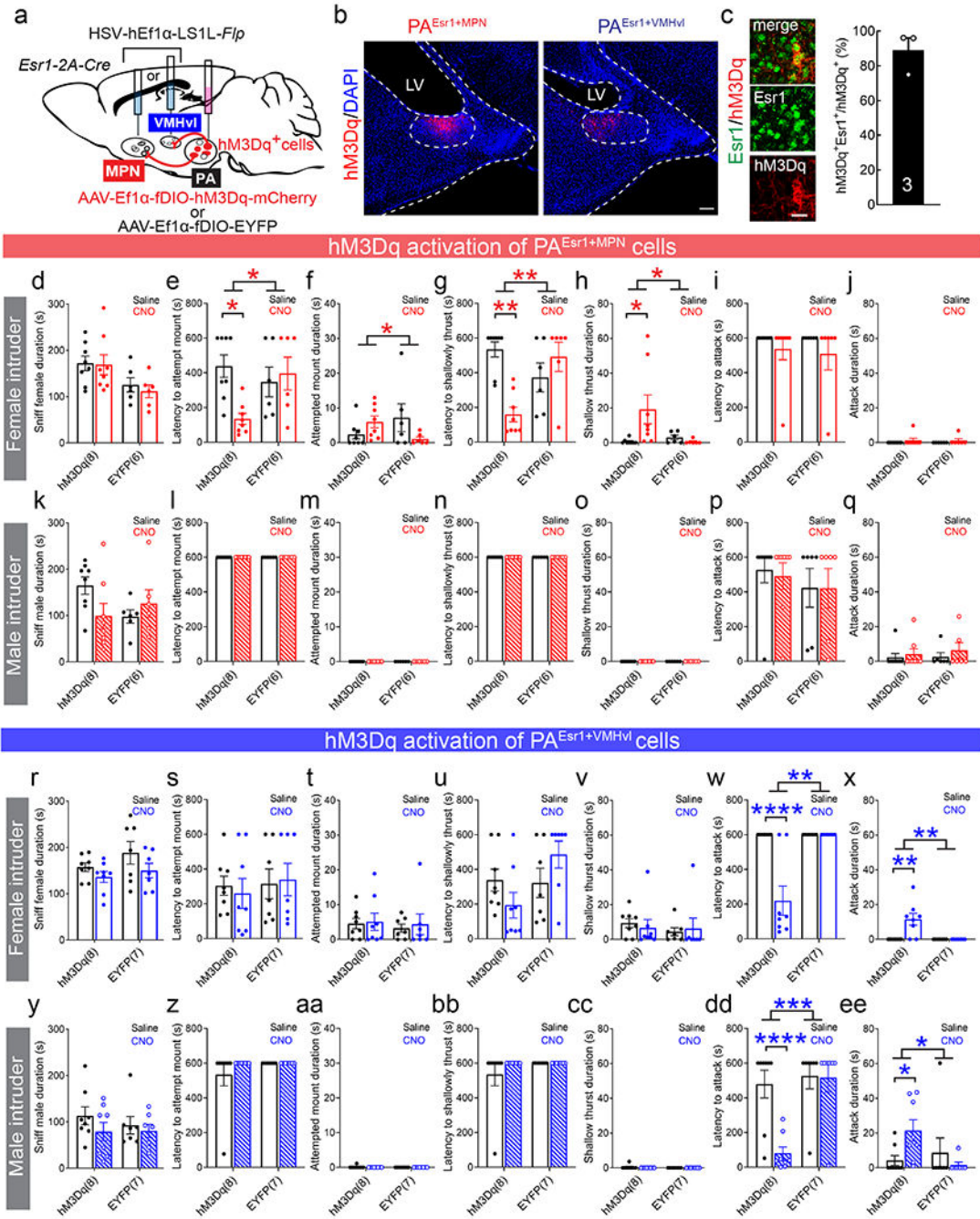
(a) Experimental schematics. (b) Representative images showing fiber tracks (yellow lines) and GCaMP6f (green) expression in PA<sup>Esr1+MPN</sup> (left) and PA<sup>Esr1+VMHvl</sup> cells (right). Blue: DAPI. Scale bar: 200 μm. (c) Representative images showing the overlap of GCaMP6f (green) and Esr1 (red) in the PA. Blue: DAPI. Scale bar: 20 μm. Right shows the percentage of GCaMP6f<sup>+</sup> neurons expressing Esr1. Data are presented mean ± s.e.m; n = 3 animals. (d and e) Representative Ca<sup>2+</sup> traces of PA<sup>Esr1+MPN</sup> cells during interaction with a female (d)

and a male (**e**) intruder. Colored shading marks behavioral episodes. (**f-n**) Peri-event histograms (PETHs) of  $\text{Ca}^{2+}$  signal of  $\text{PA}^{\text{Esr1+MPN}}$  cells aligned to intruder introduction and onsets of various social behaviors. Gray and color lines represent data from individual animals and the population average.  $n = 7$  animals but only 5 animals showed attack. (**o** and **p**) Representative  $\text{Ca}^{2+}$  traces of  $\text{PA}^{\text{Esr1+VMHvl}}$  neurons during interaction with a female (**o**) and a male (**p**) intruder. (**q-y**) PETHs of  $\text{Ca}^{2+}$  signal of  $\text{PA}^{\text{Esr1+VMHvl}}$  cells aligned to intruder introduction and onsets of various social behaviors. (**z**) Peak  $\text{Ca}^{2+}$  signal of  $\text{PA}^{\text{Esr1+MPN}}$  and  $\text{PA}^{\text{Esr1+VMHvl}}$  cells during introduction and investigation of social and non-social stimuli, and during various stages of sexual behaviors and attack.  $n = 7$  animals except attack ( $n = 5$  animals) in  $\text{PA}^{\text{Esr1+MPN}}$  group.  $n = 5$  animals in  $\text{PA}^{\text{Esr1+VMHvl}}$  group. All data in **z** are presented as mean  $\pm$  s.e.m. One-way ANOVA with Tukey multiple comparison test. \* $p < 0.05$ , \*\* $p < 0.01$ , \*\*\* $p < 0.001$ . See also Extended Data Fig. 3, 4, 5, 6. For detailed statistics information, see Supplementary Table 1.



**Figure 5. Pharmacogenetic inhibition of PA<sup>Esr1+MPN</sup> and PA<sup>Esr1+VMHvl</sup> cells impairs sexual and aggressive behaviors**  
**(a)** Experimental schematics. **(b)** Representative images showing hM4Di (red) expression in PA<sup>Esr1+MPN</sup> (left) and PA<sup>Esr1+VMHvl</sup> cells (right). Blue: DAPI. Scale bar: 200  $\mu$ m. **(c)** Representative images showing overlap between hM4Di (red) and Esr1 (green) in the PA. Scale bar: 20  $\mu$ m. Right shows the percentage of hM4Di positive neurons expressing Esr1.  $n = 3$  animals. **(d-j)** Sexual behaviors are significantly impaired after PA<sup>Esr1+MPN</sup> inactivation. Duration of female investigation **(d)** significantly increased after CNO injection in test group

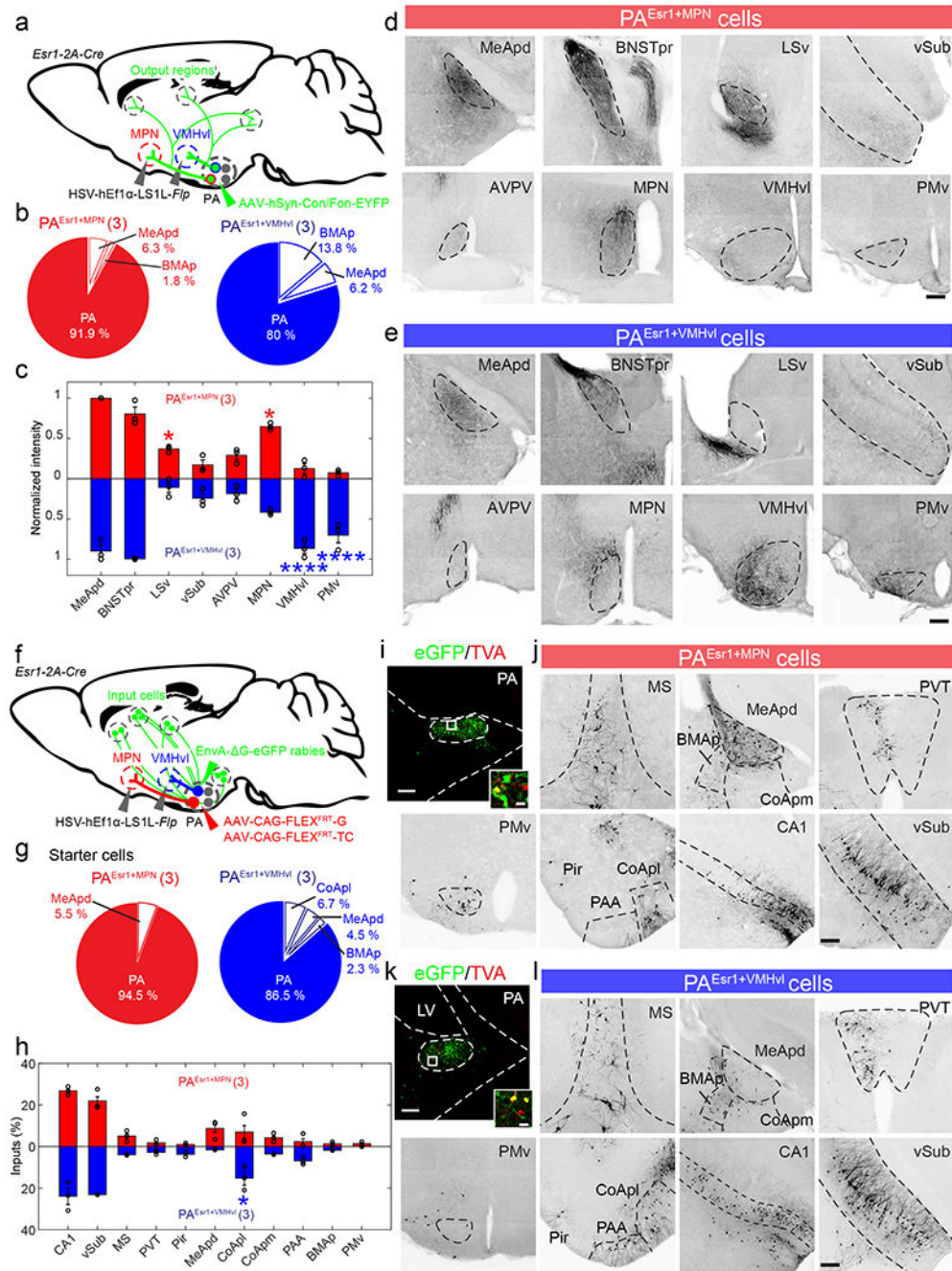
but not control group. Latencies to attempted mounting (**e**), shallow thrust (**g**) and deep thrust (**i**) increase while durations of attempted mounting (**f**), shallow thrust (**h**) and deep thrust (**j**) decrease after CNO injection in test group but not control group. (**k-m**)  $PA^{Esr1+MPN}$  inactivation does not impair aggressive behaviors towards males.  $n = 8$  (hM4Di) and 6 (EYFP) animals in **d-m**. (**n-w**) Comparison of social investigation, sexual and aggressive behaviors after CNO and saline injections in animals expressing hM4Di in  $PA^{Esr1+VMHvl}$  cells. Latency to deep thrust (**s**) significantly increases in test group after CNO. Duration of deep thrust (**t**) and duration of attack (**w**) significantly decrease after CNO injection in test but not control groups.  $n = 8$  (hM4Di) and 5 (EYFP) animals in **n-w**. Each test lasts 10 minutes. For animals that did not show the relevant behavior within the testing period, the latency will be set at 600s. All data in **d-w** are presented as mean  $\pm$  s.e.m. Two-way ANOVA with repeated measures followed by Bonferroni's multiple comparison test. \* $p < 0.05$ , \*\* $p < 0.01$ , \*\*\* $p < 0.001$ , \*\*\*\* $p < 0.0001$ . See also Extended Data Fig. 7. For detailed statistics information, see Supplementary Table 1.



**Figure 6. Pharmacogenetic activation of PA<sup>Esr1+MPN</sup> and PA<sup>Esr1+VMHvl</sup> cells differentially promote sexual and aggressive behaviors in naïve males.**

(a) Experimental schematics. (b) Representative images showing hM3Dq (red) expression in PA<sup>Esr1+MPN</sup> (left) and PA<sup>Esr1+VMHvl</sup> cells (right). Blue: DAPI. Scale bar: 200 μm. (c) Representative images showing overlap between hM3Dq (red) and Esr1 (green) in the PA. Scale bar: 20 μm. Right shows the percentage of hM3Dq positive neurons expressing Esr1. n = 3 animals. (d-j) Sexual behaviors in naïve males towards non-receptive females are significantly enhanced after PA<sup>Esr1+MPN</sup> activation. Duration of female investigation (d)

shows no change after CNO injection in both test group and control group. Latencies to attempted mounting (**e**) and shallow thrust (**g**) decreased while durations of attempted mounting (**f**) and shallow thrust (**h**) increased after 0.1 mg/kg CNO injection in test group but not control group. (**k-q**) 0.1 mg/kg CNO injection does not change social investigation towards male and aggressive behaviors towards males or females in PA<sup>Esr1+MPN</sup> hM3Dq expressing or control animals. n = 8 (hM3Dq) and 5 (EYFP) animals in **d-q**. (**r-ee**) Aggressive but not sexual behaviors in naïve males towards both males and females increased after PA<sup>Esr1+VMHvl</sup> activation. 0.5mg/kg CNO injection did not change investigatory or sexual behaviors (**r-v**, **y-cc**) while significantly shortened attack latency (**w** and **dd**) and increased attack duration (**x** and **ee**) towards both male and female intruders. n = 8 (hM3Dq) and 5 (EYFP) animals in **r-ee**. Note that after saline injection, no male attacked female and only 2/8 attacked male while 6/8 attacked female and all attacked male intruders after CNO injection. Each test lasts 10 minutes. For animals that did not show the relevant behavior within the testing period, the latency will be set at 600s. All data in **d - ee** are presented as mean ± s.e.m. Two-way ANOVA with repeated measures followed by Bonferroni's multiple comparison test. \*p < 0.05, \*\*p < 0.01, \*\*\*p<0.001, \*\*\*\*p< 0.0001. See also Extended Data Figs. 8, 9. For detailed statistics information, see Supplementary Table 1.



viral strategy for labeling the direct upstream cells of PA<sup>Esr1+MPN</sup> or PA<sup>Esr1+VMHvl</sup> populations. FLEX<sup>FRT</sup>, *Ffp*-dependent expression; G, rabies glycoprotein; TC, TVA-mCherry fusion. (g) Pie charts show the distributions of all starter cells. n = 3 animals for each group. (h) Distributions of the cells upstream of PA<sup>Esr1+MPN</sup> and PA<sup>Esr1+VMHvl</sup> cells. n = 3 animals for each group. (i and k) Images showing the starter cells in the PA (yellow) and neighboring PA neurons that project to the starter cells (green). Insets showing the enlarged view of the box areas. Scale bars: 200  $\mu$ m and 20  $\mu$ m (insets). (j and l) Representative images showing the rabies labeled cells in various brain regions, presumably upstream of PA<sup>Esr1+MPN</sup> (j) and PA<sup>Esr1+VMHvl</sup> (l) populations. Scale bars = 200  $\mu$ m. Images in d, e, and i-l are representative of n = 3 mice. All data in c and h are presented as mean  $\pm$  s.e.m; Two-way ANOVA followed by with Bonferroni's multiple comparison test. \*p < 0.05, \*\*p < 0.01. See also Extended Data Fig. 10. For detailed statistics information, see Supplementary Table 1.